AD-A052 290 WASHINGTON UNIV SEATTLE DEPT OF ELECTRICAL ENGINEERING F/G 20/6
OPTICAL PROPERTIES OF SINGLE MODE RECTANGULAR FIBERS.(U)
FEB 78 C A KOHAN, G L MITCHELL, S S YEE N00123-76-C-1451
UNCLASSIFIED UW-EE-TR-207 NL

1 OF
AD
A052 290

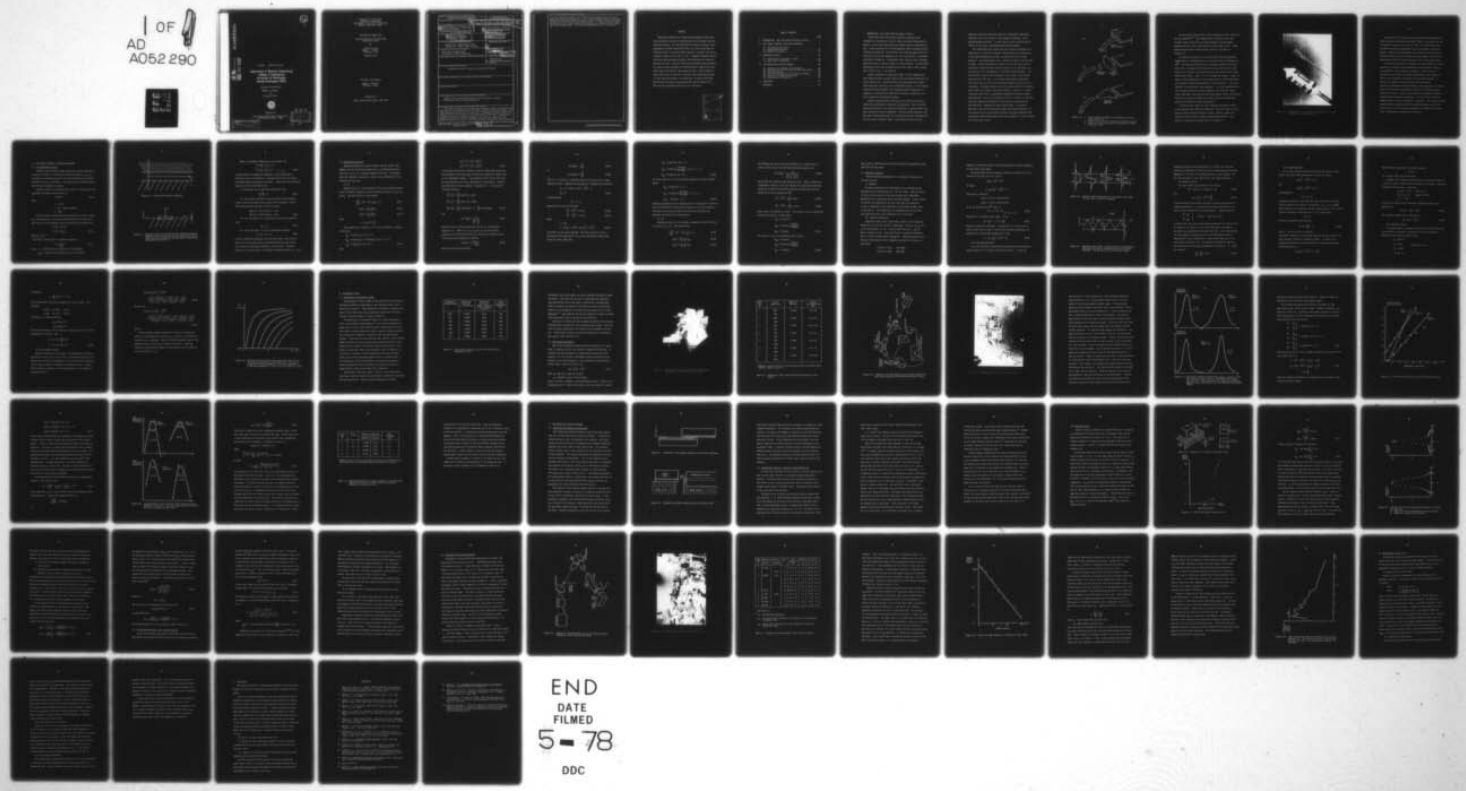

END
DATE
FILMED
5-78
DDC

(12)

Contract N00123-76-C-1451

Department of Electrical Engineering
College of Engineering
University of Washington
Seattle, Washington 98195

Principal Investigators

GORDON L. MITCHELL

and

WILLIAM D. SCOTT

Prepared for

Naval Ocean Systems Center (Code 8115)
San Diego, California 92152

University of Washington
College of Engineering
Department of Electrical Engineering
Seattle, Washington 98195

EE Technical Report 207

Optical Properties of Single Mode Rectangular Fibers

by

Carlos A. Kohan
Gordon L. Mitchell
Sinclair S. Yee

February 1978

Principal Investigators

Gordon L. Mitchell
William D. Scott

Prepared for

Naval Ocean Systems Center, Code 8115

SECURITY CLASSIFICATION OF THIS PAGE (When Data Entered)

REPORT DOCUMENTATION PAGE	READ INSTRUCTIONS BEFORE COMPLETING FORM
1. REPORT NUMBER	2. GOVT ACCESSION NO. (9) Final Rept. 1 Jun 76-31 Dec 78, 3. RECIPIENT'S CATALOG NUMBER
4. TITLE (and Subtitle) (6) Optical Properties of Single Mode Rectangular Fibers •	5. TYPE OF REPORT & PERIOD COVERED Final 6/1/76 - 12/31/78
	(14) 6. PERFORMING ORG. REPORT NUMBER UW EE-TR-207
7. AUTHOR(s) (10) Carlos A. Kohan, Gordon L. Mitchell Sinclair S. Yee	8. CONTRACT OR GRANT NUMBER(s) (15) N00123-76-C-1451
9. PERFORMING ORGANIZATION NAME AND ADDRESS University of Washington (FT-10) Seattle, WA 98195 (206) 543-2185	10. PROGRAM ELEMENT, PROJECT, TASK AREA & WORK UNIT NUMBERS (11)
11. CONTROLLING OFFICE NAME AND ADDRESS Naval Ocean Systems Center San Diego, CA 92152 (Code 8115)	12. REPORT DATE Feb 78 13. NUMBER OF PAGES 71 (12) 73 p.
14. MONITORING AGENCY NAME & ADDRESS (if different from Controlling Office)	15. SECURITY CLASS. (of this report) UNCLASSIFIED 15a. DECLASSIFICATION/DOWNGRADING SCHEDULE

16. DISTRIBUTION STATEMENT (of this Report)

Approved for public release; distribution unlimited

17. DISTRIBUTION STATEMENT (of the abstract entered in Block 20, if different from Report)

18. SUPPLEMENTARY NOTES

19. KEY WORDS (Continue on reverse side if necessary and identify by block number)

optical fibers, single-mode fibers, optical coupling, coupling efficiency, fiber or integrated optics

20. ABSTRACT (Continue on reverse side if necessary and identify by block number)

The optical properties of single-mode rectangular fibers have been studied with the aim of improving past DH laser/fiber coupling efficiency results. By local heating and careful fracturing, short, rectangular-to-round "transition" fibers can later be obtained for efficient overall laser/round fiber coupling. The power loss due to rounding is known to be as low as 1 dB. A method of general applicability has been developed to measure core dimensions and numerical aperture of fibers. Coupling efficiency measurements were performed

DD FORM 1 JAN 73 1473 EDITION OF 1 NOV 65 IS OBSOLETE S/N 0102 LF 014 6601

400 915

SECURITY CLASSIFICATION OF THIS PAGE (When Data Entered)

by a more reliable procedure for differentiating cladding from core output power than what has been generally used. Laser/rectangular fiber efficiencies of 30% with a maximum of 50% have been obtained. If laser fluorescent power is accounted for to compare with other publications, the above figures become 46% and 71% respectively. This work was supported by N.S.F. and N.O.S.C.

ABSTRACT

The optical properties of single-mode rectangular fibers have been studied with the aim of improving past DH laser/fiber coupling efficiency results. By local heating and careful fracturing, short, rectangular-to-round "transition" fibers can later be obtained for efficient overall laser/round fiber coupling. The power loss due to rounding is known to be as low as 1 dB. A method of general applicability has been developed to measure core dimensions and numerical aperture of fibers. Coupling efficiency measurements were performed by a more reliable procedure for differentiating cladding from core output power than what has been generally used. Laser/rectangular fiber efficiencies of 30% with a maximum of 50% have been obtained. If laser fluorescent power is accounted for to compare with other publications, the above figures become 46% and 71% respectively.

This work was supported jointly by N.S.F. and N.O.S.C.

TABLE OF CONTENTS

1. INTRODUCTION - Why Single-Mode Rectangular Fibers?

Single-mode fibers have several potential advantages when considered as transmission lines for high rate optical communication systems. On one hand they provide the highest possible bandwidths to date. Pulse distortion of an electromagnetic signal propagating along a dielectric waveguide results mainly from different group velocities along the direction of propagation (z) due to two factors: intermodal and material dispersion. Single-mode fibers naturally lack intermodal dispersion which is the most serious of these problems. The attainable bandwidth has thus been estimated to be on the order of tens of gigahertz (10^9 Hz) over a 1 km distance.

Another advantage of single-mode fibers is their compatibility with integrated optics systems which can provide advanced modulator and switch capabilities. Multimode fibers have been shown to be highly inefficient when coupling to such single-mode systems. In this respect single-mode fibers together with integrated optical components are expected to constitute the communication channels of high data rate, large information distribution systems.

Several problems however remain yet to be solved for practical single-mode communication systems to be realizable. One of the most serious difficulties is the coupling efficiency, or optical power loss when connecting different components. The two guiding geometries that have been studied extensively are the thin-film (planar) waveguide and the well known cylindrical fiber. Much research effort has been

directed to coupling efficiency studies of single-mode fiber/fiber, fiber/thin-film, thin-film/thin-film waveguide interfaces, and of source/waveguide coupling[1]. In this report we have concentrated our efforts on the crucial source/waveguide coupling problem.

For single-mode fiber systems the most promising candidate for a light source, in view of its optical characteristics and reliability, is the double heterostructure (DH), cw injection laser of stripe geometry[2]. Its output however has a strongly elliptical cross sectional shape. Typical dimensions are about 13 μm for the major axis of the ellipse, along the plane of the pn junction (yz), and about 1 μm for the minor axis, perpendicular to the plane of the junction. This field pattern is due to the rectangular cross section of the active area (stripe) of the laser. On the other hand typical single-mode fiber cores have a circular cross sectional shape of about 3 to 6 μm in diameter. Bringing a fiber close to the active area of an injection laser results in a highly inefficient coupling. Figure 1-1.a clearly illustrates that there is considerable geometrical mismatch between both apertures. As will be discussed in detail in Section 4, coupling efficiency depends on matching the field pattern distributions of both apertures. Assuming all other factors ideal, i.e., perfect matching of the field distributions along the plane perpendicular to the junction (xz), we can estimate based on the above geometries that the highest coupling efficiences that can be expected in this situation are of the order of 25%.

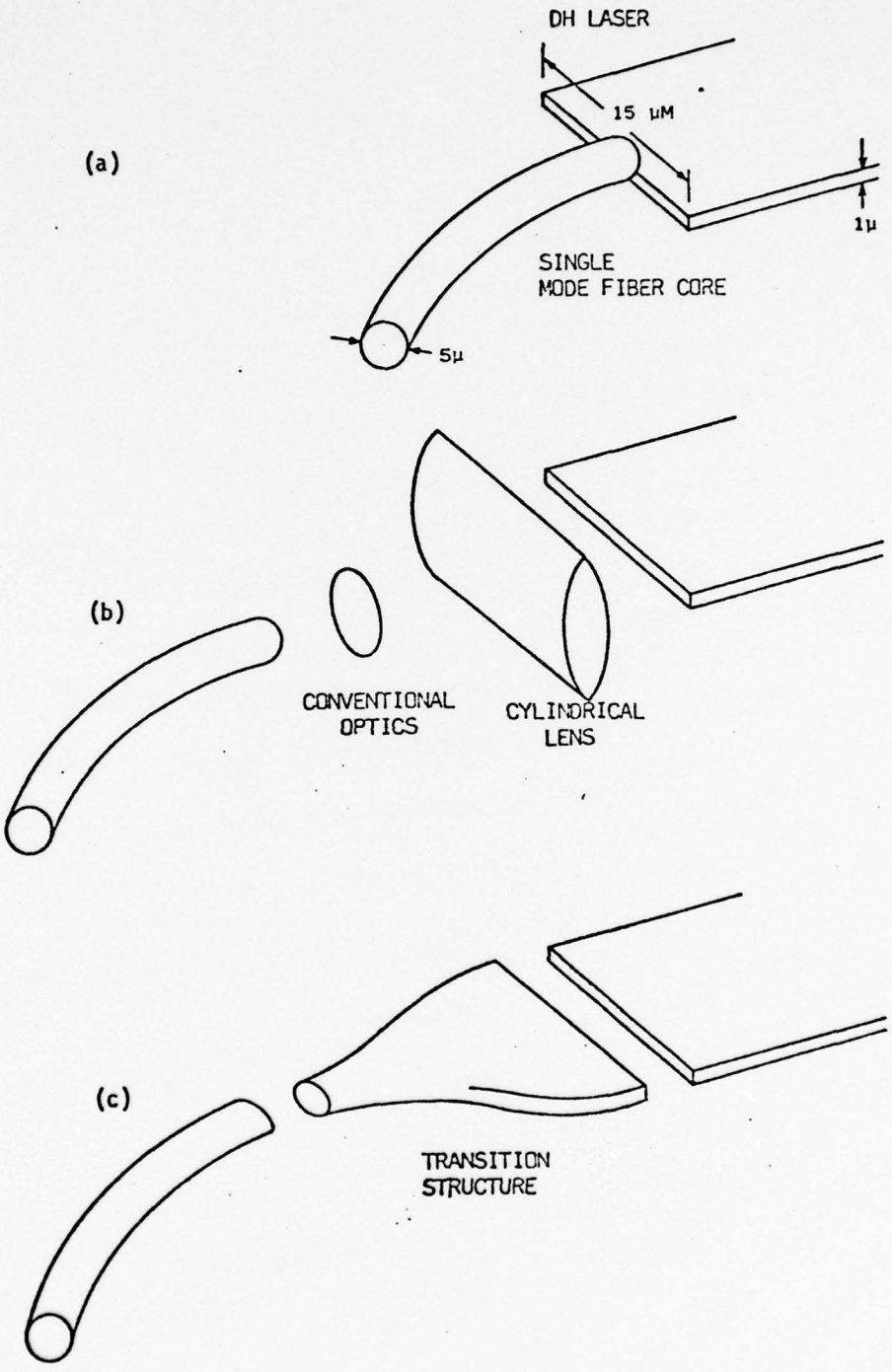

Figure 1-1. a. Direct coupling between a DH injection laser and a single-mode fiber
b. Typical hybrid optical structures studied to present.
c. Laser/fiber coupling through a rectangular-to-round transition fiber.

To the present, experimental results presented by other researchers are not conclusive[3-7]. Even though higher efficiencies have been claimed, typical values for this direct end-butt coupling method between a DH laser and a round fiber are on the order of 10%. A more detailed discussion of these previous results is presented in Section 4.2.

An alternative approach to the laser/fiber coupling problem was suggested by D. G. Dalgoutte et al. at the University of Washington in 1975[8]. The idea was to fabricate a single-mode, tapered "transition" fiber with a rectangular cross section on one end to match the laser output, and a circular cross section on the other end to match regular transmission fibers. Figure 1-1.c illustrates the concept. Figure 1-2 shows an actual photograph of one of such transition fibers fabricated at the Ceramic Engineering Department of this University. A 1/4 watt resistor is also shown for size comparison. If a high laser/transition fiber coupling efficiency could be obtained, the transition fiber/round single-mode fiber coupling should not present serious difficulties. Fiber/fiber coupling efficiencies as high as 94% have already been measured consistently by other researchers[1].

The fabrication process for this transition structure involves first obtaining long ribbons of rectangular fibers and later by local heating allowing certain sections to round. Finally, cleanly cut pieces are obtained under carefully controlled conditions. This process is discussed in greater detail in Section 3.1.

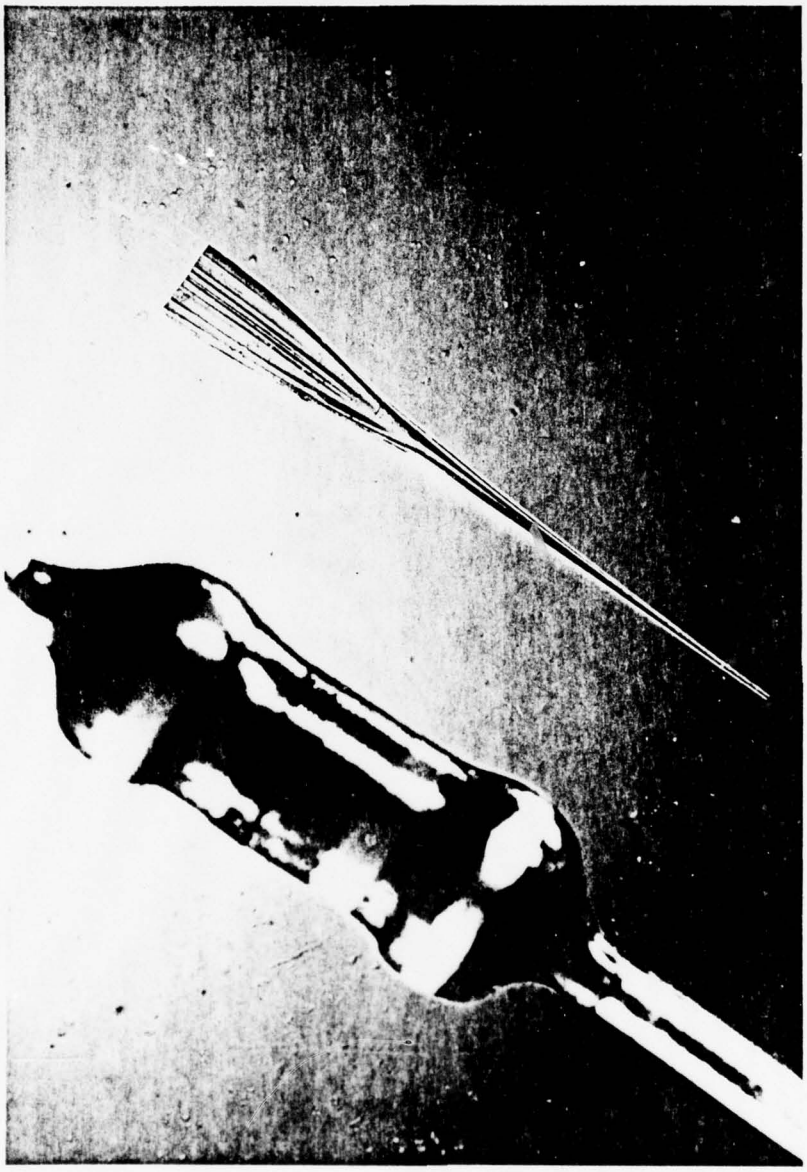

Figure 1-2. Photograph of a transition fiber shown by a 1/4 watt resistor for size comparison.

The purpose of this work was to study the optical properties of these ribbons of single-mode rectangular fibers, since power loss due to rounding is known to be as low as 1 dB. In a joint effort with the Ceramic Engineering Department, sets of rectangular fibers were pulled. Several glass combinations with different refractive index relations between core and cladding have been tested. The aim was to experimentally optimize laser/rectangular fiber coupling efficiency.

In Section 2 we present a summary of the basic theoretical results necessary to understand the propagation of electromagnetic radiation in a symmetric, planar dielectric waveguide. These results are essential to understand the problems encountered in our research as well as the experimental techniques that have been employed. In Section 3 we summarize the fiber fabrication process and discuss an experimental method developed in this laboratory to actually measure core thickness and numerical aperture (core/cladding index relation) of fibers. Section 4 deals with the fundamental problem of coupling light between two waveguides. A brief critical review of present results by other researchers is presented. Our source measured characteristics, coupling efficiency measuring system, results and difficulties are also discussed, together with suggestions for future work. Conclusions are presented in Section 5.

2. THE PLANAR, SYMMETRIC, DIELECTRIC WAVEGUIDE

2.1 The Fundamental Problem

Consider three dielectric media with planar parallel boundaries, as shown in Figure 2-1, and optical refractive indices n_1, n_2, n_3.[†] The choice of coordinate system is such that these media are assumed unbounded in the y,z directions. This convention for coordinate axes will be used throughout this report.

We will consider time harmonic fields, that is fields with a time dependence in complex notation given by

$$\exp(i\omega t) \tag{2-2}$$

where

$$i = (-1)^{\frac{1}{2}}$$

$$\omega = 2\pi f \quad \text{angular frequency}$$

$$t = \text{time.}$$

We will further assume the dielectric media to be linear, isotropic, and homogeneous. Under these conditions Maxwell's equations[9] then reduce to two independent vector equations for each medium (j):

$$\vec{\nabla} \times \vec{\mathcal{E}}_j = -i\omega\mu_j \vec{H}_j$$

$$\vec{\nabla} \times \vec{H}_j = i\omega\varepsilon_j \vec{\mathcal{E}}_j \tag{2-3}$$

with j = 1, 2, 3.

[†] The index of refraction of a medium is defined as

$$n = \left(\frac{\varepsilon\mu}{\varepsilon_o\mu_o}\right)^{\frac{1}{2}} \tag{2-1}$$

where ε,μ: permittivity and permeability of the medium

ε_o,μ_o: permittivity and permeability of free space.

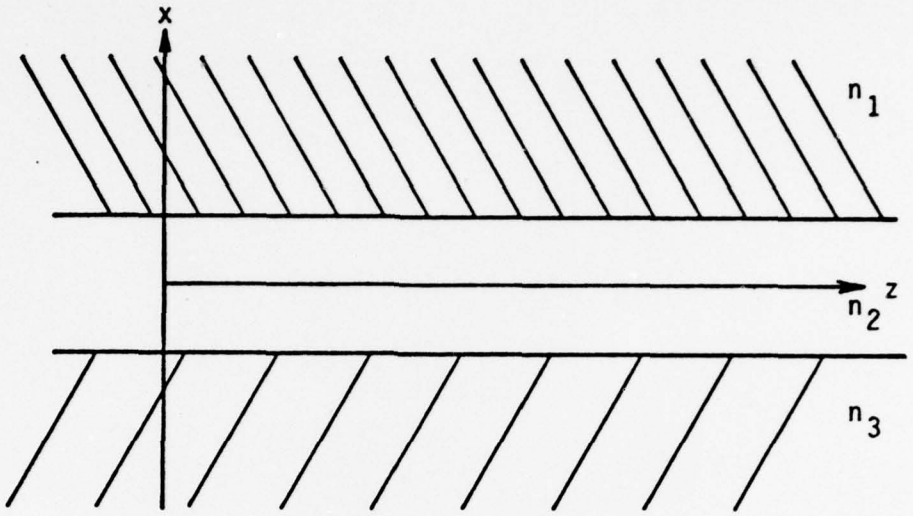

Figure 2-1. The planar dielectric waveguide.

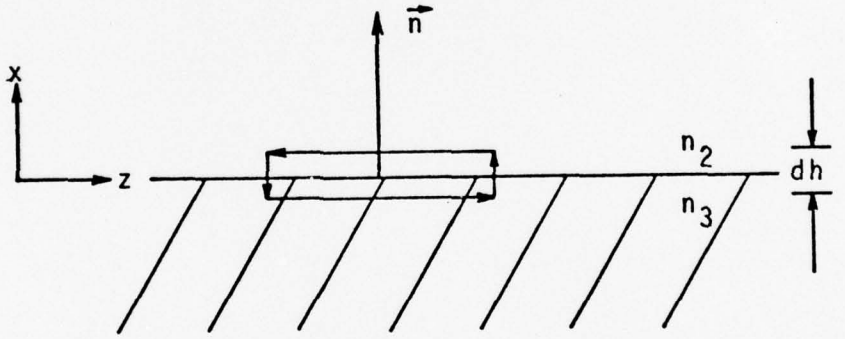

Figure 2-2. Boundary conditions are obtained by integrating Maxwell's equations over a rectangular area of differential height (dh) across the boundary, using then Stoke's theorem and taking the limit as $dh \to 0$.

Hence, the boundary conditions are (see Figure 2-2)

$$\vec{n} \times (\vec{H}_j - \vec{H}_{j+1}) = 0$$

$$\vec{n} \times (\vec{\mathcal{E}}_j - \vec{\mathcal{E}}_{j+1}) = 0 \qquad j = 1, 2 \tag{2-4}$$

In other words, the tangential components of the fields must be continuous across the boundaries. Equations (2-3) and (2-4) define our problem under very general conditions. Actually for our particular problem we will be more restrictive:

i) Since there are no variations along the y axis,

$$\frac{\partial}{\partial y} \left\{ \begin{matrix} \vec{\mathcal{E}} \\ \vec{H} \end{matrix} \right\} = 0 \tag{2-5}$$

ii) We are only interested in those solutions that represent a wave travelling through medium 2 along the +z direction. We are thus restricting the solutions to be of the form:

$$\vec{\mathcal{E}}(x,z,t) = \vec{E}(x) \exp[i(\omega t - \beta z)]$$

$$\vec{H}(x,z,t) = \vec{H}(x) \exp[i(\omega t - \beta z)] \tag{2-6}$$

iii) For our purposes it is sufficient to solve the symmetric case,

$$n_1 = n_3 \tag{2-7}$$

iv) As in most cases, it is also valid here to assume:

$$\mu_1 = \mu_2 = \mu_3 = \mu_o \tag{2-8}$$

It may be noted from equations (2-4) and (2-6) that ω and β must be equal in all three media since the boundary conditions must be met at all points on the planar interfaces, for any time. The phase velocity of the wave along z is obtained from equation (2-6) as $v = \omega/\beta$.

2.2 Guided Mode Solutions

Waveguide problems are usually divided into two simpler independent ones by alternatively imposing $E_z = 0$, transverse electric (TE) case, and $H_z = 0$, transverse magnetic (TM) case. The general solution to Maxwell's equations is then a linear combination of the solutions for each case.

i) TE

Assuming $E_z(x) = 0$, from equations (2-3) and our previous assumptions the nonzero components of the fields may be shown to be E_y, H_x, and H_z. They must satisfy in each medium:

$$\left[\frac{\partial^2}{\partial x^2} + (k^2 - \beta^2)\right] E_y(x) = 0 \qquad (2\text{-}9)$$

$$H_x(x) = \frac{1}{i\omega\mu} \frac{\partial}{\partial z}(E_y) \qquad (2\text{-}10)$$

$$H_z(x) = \frac{-1}{i\omega\mu} \frac{\partial}{\partial x}(E_y) \qquad (2\text{-}11)$$

where

$$k = \omega(\varepsilon\mu)^{\frac{1}{2}} = \frac{2\pi}{\lambda} .$$

Since there are no sources at $x = \pm\infty$, we can propose a solution of the form:

$$E_{1y} = A \exp(-ip_1 x), \text{ for } x \geq d$$

$$E_{2y} = B \exp(-ip_2 x) + C \exp(ip_2 x), \text{ for } d \geq x \geq -d$$

$$E_{3y} = D \exp(ip_1 x), \text{ for } -d \geq x \qquad (2\text{-}12)$$

with

$$p_1^2 + \beta^2 = k_1^2 = k_o^2 n_1^2$$
$$p_2^2 + \beta^2 = k_2^2 = k_o^2 n_2^2 \qquad (2\text{-}13)$$

In the above solutions the constant β and all coefficients except one, which depends on the total power and which we arbitrarily choose to be A, are independent unknowns. From equations (2-11) and (2-12) we can get the expressions for the H_z components for each region. Imposing now continuity of these tangential components at $x = \pm d$ we get the following equations:

$$\frac{B}{A} = \frac{1}{2}\left(1 + \frac{p_1}{p_2}\right) \exp[i(p_2 - p_1)d]$$

$$\frac{C}{A} = \frac{1}{2}\left(1 - \frac{p_1}{p_2}\right) \exp[-i(p_1 + p_2)d]$$

$$\frac{D}{A} = \frac{1}{2}i\left(1 + \frac{p_1}{p_2}\right) \exp(2ip_2 d) + \left(1 - \frac{p_1}{p_2}\right) \exp(-2ip_2 d)] \qquad (2\text{-}14)$$

and

$$\tan(2p_2 d) = \frac{2i}{\frac{p_2}{p_1} + \frac{p_1}{p_2}} \qquad (2\text{-}15)$$

Equation (2-15) if used together with (2-13) is a trascendental equation in β. Indeed if n_1, n_2, k_o (or λ_o), and d are fixed, equation (2-15) gives those values of β for which a solution exists. If we now use the trigonometric identity

$$\tan(2\alpha) = \frac{2\tan\alpha}{1 - \tan^2\alpha} \qquad (2\text{-}16)$$

We get two sufficient equations

$$\tan (p_2 d) = i \frac{p_1}{p_2} \tag{2-17}$$

or

$$\tan (p_2 d) = i \frac{p_2}{p_1} \tag{2-18}$$

That is, if a value of β satisfies either (2-17) or (2-18), it then satisfies (2-15). Imposing now the guided or "trapped" wave condition:

$$p_1 = -i\alpha, \text{ with } \alpha = (\beta^2 - k_1^2)^{\frac{1}{2}} > 0$$

$$p_2 > 0 \tag{2-19}$$

or equivalently

$$k_2 > \beta > k_1$$

Equations (2-17) and (2-18) become

$$(a^2 - u^2)^{\frac{1}{2}} = u \tan u \tag{2-20}$$

$$(a^2 - u^2)^{\frac{1}{2}} = -u \cot u \tag{2-21}$$

where

$$u = p_2 d$$

$$a = d (k_2^2 - k_1^2)^{\frac{1}{2}} = k_o d (n_2^2 - n_1^2)^{\frac{1}{2}} \tag{2-22}$$

The fields are now easily obtained. For those values of u (or β) satisfying (2-20) equations (2-14) can be rearranged to obtain from (2-12) the field expressions

$$E_{1y} = A \exp(-\alpha x), \text{ for } x \geq d$$

$$E_{2y} = A \exp(-\alpha d) \frac{\cos (p_2 x)}{\cos (p_2 d)}, \text{ for } d \geq x \geq -d$$

$$E_{3y} = A \exp(\alpha x), \text{ for } -d \geq x \qquad (2\text{-}23)$$

For those values of u (or β) satisfying equation (2-21) we similarly obtain

$$E_{1y} = A \exp(-\alpha x), \; x \geq d$$

$$E_{2y} = A \exp(-\alpha d) \frac{\sin (p_2 x)}{\sin (p_2 d)}, \; d \geq x \geq -d$$

$$E_{3y} = -A \exp(\alpha x), \; -d \geq x \qquad (2\text{-}24)$$

Although unnecessary, we have purposely kept all constants to explicitly show the continuity of the E_y field component across the boundaries. The values of H_x and H_z for each case are easily obtained from equations (2-10) and (2-11) respectively.

ii) TM

Assuming now $H_z(x) = 0$, the nonzero components of the fields turn out to be H_y, E_x, E_z. They must satisfy

$$\left[\frac{\partial^2}{\partial x^2} + (k^2 - \beta^2)\right] H_y(x) = 0 \qquad (2\text{-}25)$$

$$E_x(x) = \frac{-1}{i\omega\epsilon} \frac{\partial}{\partial z} (H_y) \qquad (2\text{-}26)$$

$$E_z(x) = \frac{1}{i\omega\epsilon} \frac{\partial}{\partial x} (H_y) \qquad (2\text{-}27)$$

By following now exactly the same procedure as for the TE case we arrive in this case at the following eigenvalue equation in β

$$\tan(2p_2 d) = \frac{2i}{\frac{p_2}{p_1}\frac{\varepsilon_1}{\varepsilon_2} + \frac{p_1}{p_2}\frac{\varepsilon_2}{\varepsilon_1}} \tag{2-28}$$

We may note the similarity with equation (2-15). Using as before the trigonometric identity (2-16) and imposing the guided mode conditions (2-19) we now obtain the following equations (one of which must be satisfied to satisfy equation (2-28))

$$(a^2 - u^2)^{\frac{1}{2}} = \left(\frac{\varepsilon_1}{\varepsilon_2}\right) u \tan u \tag{2-29}$$

$$(a^2 - u^2)^{\frac{1}{2}} = -\left(\frac{\varepsilon_1}{\varepsilon_2}\right) u \cot u \tag{2-30}$$

where a and u are defined in (2-22). For values of u (or β) satisfying (2-29) we now obtain, in each region

$$\begin{aligned} H_{1y} &= A \exp(-\alpha x) \\ H_{2y} &= A \exp(-\alpha d) \frac{\cos(p_2 x)}{\cos(p_2 d)} \\ H_{3y} &= A \exp(\alpha x) \end{aligned} \tag{2-31}$$

For values of u (or β) satisfying (2-30) we obtain

$$\begin{aligned} H_{1y} &= A \exp(-\alpha x) \\ H_{2y} &= A \exp(-\alpha d) \frac{\sin(p_2 x)}{\sin(p_2 d)} \\ H_{3y} &= -A \exp(\alpha x) \end{aligned} \tag{2-32}$$

The E_x and E_z components are now easily obtained from equations (2-26) and (2-27) for each case.

2.3 Analysis of Results

From the preceding derivation, it is important to observe the following results

i) Symmetry

As may be expected due to the symmetry of our problem we have obtained even and odd functions of x for the fields. They all follow a sine or cosine function in the core region, with a decreasing exponential tail (evanescent field) into the cladding. It may further be noticed from equations (2-10) and (2-26) that the transverse (x and y) components of the fields have in each case the same (even or odd) parity. The longitudinal (z) components have on the other hand opposite parity to the transverse ones in all cases.

ii) Eigenvalue Equations

Equations (2-20), (2-21), and (2-29), (2-30) are the eigenvalue equations for the TE and TM cases respectively. Given n_1, n_2, d, and λ_o (or equivalently ω or k_o), they give the values of $u = p_2 d$ for which a solution exists. Each such value of u naturally determines what is called a guided mode of propagation. Referring always to the parity of the transverse field components we obtain, for values of u satisfying:

(2-20) or (2-29)	even modes
(2-21) or (2-30)	odd modes

Figure 2-3 illustrates typical distribution patterns of these components for the lowest order modes.

It may be noted that the eigenvalue equations represent the intersection of the upper half of a circle:

$$y_c(u) = (a^2 - u^2)^{\frac{1}{2}}$$

of radius

$$a = k_o\, d(n_2^2 - n_1^2)^{\frac{1}{2}} \geq 0$$

with curves of the form

$$y_1(u) \propto u \tan u, \text{ even solutions}$$

$$y_2(u) \propto u \cot u, \text{ odd solutions}$$

It is not difficult to see[10] that, if

$$m\pi < a < (m + 1)\pi \qquad m = 0, 1, 2, \ldots \tag{2-33}$$

there are m + 1 different even modes. If now

$$(m - \tfrac{1}{2})\pi < a < (m + \tfrac{1}{2})\pi \tag{2-34}$$

there are m different odd modes. In particular it is clear that in order to have only one even TE and one even TM mode propagating, the condition for (single-mode) propagation is then

$$a = k_o\, d(n_2^2 - n_1^2)^{\frac{1}{2}} < \frac{\pi}{2} \tag{2-35}$$

iii) The Poynting Vector

It is not difficult to verify that the direction of the Poynting vector coincides in all cases with the optical axis z. Since the

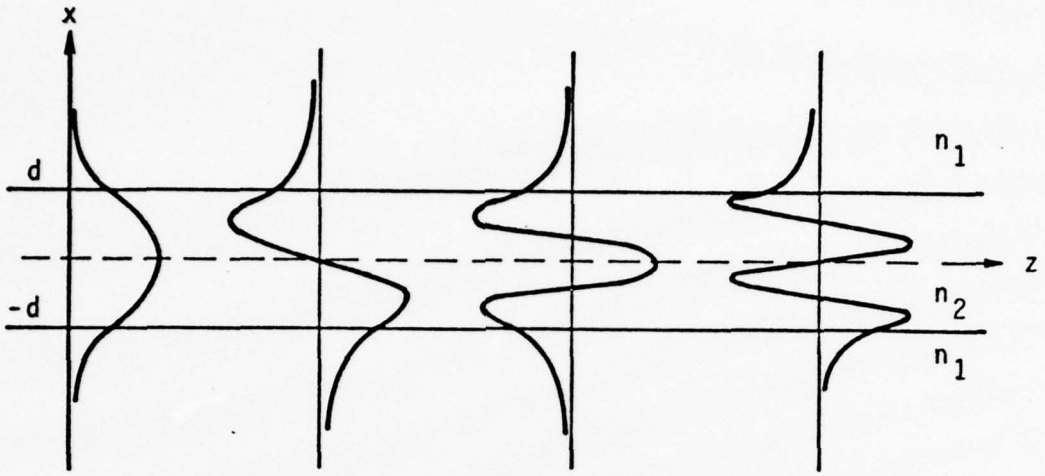

Figure 2-3. Typical field distributions for the lowest order modes for the planar, symmetric waveguide.

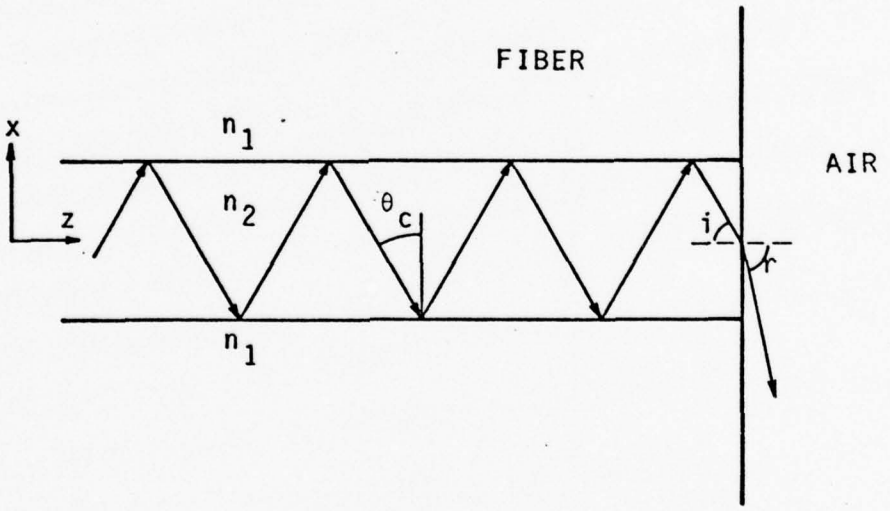

Figure 2-4. Geometric optics model. Guided modes are represented by rays which are totally reflected at the core-cladding interface. The ray shown is at the critical angle.

transverse fields have the same parity, it is then clear that the intensity distribution will follow a sine or cosine squared functional dependence in the core, with exponential tails in the cladding. We will take advantage of this conclusion in our future discussion.

iv) Geometric Optics

Let a wave vector $\vec{k}_2$ be defined in the core as

$$\vec{k}_2 = (p_2, 0, \beta) = k_o(n_x, 0, n_z) \tag{2-36}$$

with

$$n_2 = (n_x^2 + n_z^2)^{\frac{1}{2}} = \frac{k_2}{k_o} \tag{2-37}$$

If we now consider the circular functions as sums or differences of complex exponentials, it is possible to represent the fields in the core as linear combinations of two plane waves. Indeed we have for

$$\left.\begin{array}{ll} \text{TE} & E_{2y} \\ \text{TM} & H_{2y} \end{array}\right\} \quad \alpha \exp[i\omega t - ik_o(\pm n_x X + n_z Z)]$$

In other words, the field at any arbitrary position $\vec{r}$ in the core, may be thought at all times as a sum of two plane waves with equal β, but opposite p_2 components of the wave vector $\vec{k}_2$. It is then possible for this geometry, although we are far from the geometric optics approximation in most applications, to talk about light rays in the core region (see Figure 2-4). We naturally associate the vector $\vec{k}_2$ for each plane wave with the corresponding ray direction. It is then, for instance

$$\frac{\beta}{k_2} = \frac{n_z}{n_2} = \sin\theta \tag{2-38}$$

v) Cut-Off Condition

It is clear from the derived field expressions (2-23), (2-24), (2-31), and (2-32) that guided modes will exist as long as

$$k_o(n_z^2 - n_1^2)^{\frac{1}{2}} = \alpha > 0$$

and

$$k_o(n_2^2 - n_z^2)^{\frac{1}{2}} = p_2 > 0$$

or equivalently,

$$n_2 > n_z > n_1 .$$

A necessary condition is then that the index of the core be greater than the index of the cladding. Furthermore, if $n_z < n_1$, α becomes purely imaginary and radiation into the cladding occurs. The so called "cut-off" condition is obtained for $\alpha = 0$, or equivalently

$$n_z = n_1$$

In this case equation (2-38) becomes

$$\text{arc sin } (\frac{n_1}{n_2}) = \theta_c \qquad (2\text{-}39)$$

with θ_c: critical angle of reflection

The cut-off condition is thus clearly equivalent to the condition of total internal reflection of geometric optics. In terms of our eigenvalue equations the cut-off condition is easily obtained from (2-33) and (2-34) as

$$d\, k_o(n_2^2 - n_1^2)^{\frac{1}{2}} = a = N\frac{\pi}{2}$$

where N gives the parity of the cut-off mode and

$$d = \frac{t}{2}$$

is, as usual, half the core thickness.

Consider now the planar guide terminated at some point along the z axis by a planar, normal interface bounded by free space. Figure 2-4 illustrates the situation. Using now

$n_2 \sin i = \sin r$ Snell's Law

$n_2 \sin \theta_c = n_1$ equation (2-39)

$\theta_c + i = 90°$

it is easy to obtain the far field half divergence angle of the guide (r) as

$$\sin (r) = (n_2^2 - n_1^2)^{\frac{1}{2}} \qquad (2\text{-}40)$$

The numerical aperture (NA) of the guide is

$$NA = (n_2^2 - n_1^2)^{\frac{1}{2}} \qquad (2\text{-}41)$$

vi) Numerical Example

If we approximate a rectangular fiber by this planar guide model we can obtain an estimate of the values of the main parameters. Considering the following typical values

$\lambda_o = 0.85$ μm

$n_1 = 1.55$ so that NA $\simeq$ 0.16

$n_2 = 1.5582$

$d = \frac{t}{2} = 1$ μm

We then get

$$a = \frac{2\pi}{\lambda_o} d\ NA \cong 1.18 < \frac{\pi}{2}$$

So we indeed have single-mode transmission on the xz plane. From equations

(2-20) $u \cong 0.813$ for TE

(2-29) $u \cong 0.815$ for TM

Considering $u \sim 0.814$ we then get

$$p_2 \cong 0.814\ \mu m^{-1}$$

$$\alpha \cong 0.858\ \mu m^{-1}$$

The fields decrease to 1/e of their peak value about 0.73 μm from the cladding/core interface. Also

$$\theta_c = \text{arc sin } (\frac{n_1}{n_2}) \cong 84°$$

$$r = \text{arc sin } (NA) \cong 9° \qquad (2\text{-}42)$$

vii) The Asymmetric Guide

Although somewhat more complicated, the problem for the general asymmetric case ($n_1 \neq n_3$) can be solved. Circular functions are still obtained for the field distributions in the core region although they are no longer symmetric with respect to the optical axis z. Exponential decays are obtained in the cladding regions. The eigenvalue equations are now:

$$\tan [2 k_o d(n_2^2 - n_z^2)^{\frac{1}{2}}]$$

$$= \frac{(n_2^2 - n_z^2)^{\frac{1}{2}}[(n_z^2 - n_1^2)^{\frac{1}{2}} + (n_z^2 - n_3^2)^{\frac{1}{2}}]}{(n_2^2 - n_z^2) - (n_z^2 - n_1^2)^{\frac{1}{2}}(n_z^2 - n_3^2)^{\frac{1}{2}}} \qquad (2\text{-}43)$$

for TE, and

$$\tan [2 k_o d (n_2^2 - n_z^2)^{\frac{1}{2}}]$$

$$= \frac{n_2^2(n_2^2 - n_z^2)^{\frac{1}{2}}[n_3^2(n_z^2 - n_1^2)^{\frac{1}{2}} + n_1^2(n_z^2 - n_3^2)^{\frac{1}{2}}]}{n_1^2 n_3^2(n_2^2 - n_z^2) - n_2^4(n_z^2 - n_1^2)^{\frac{1}{2}}(n_z^2 - n_3^2)^{\frac{1}{2}}} \qquad (2\text{-}44)$$

for TM.

They have been purposely expressed in terms of the guide parameters to clearly show that fixed n_1, n_2, n_3 and d/λ_o, a multivalued function of n_z is obtained. Figure 2-5 shows the general shape of the typical curves n_z versus d/λ_o for given values of n_i. Equations (2-43) and (2-44) naturally reduce to the equations for the symmetric case if we allow $n_1 = n_3$.

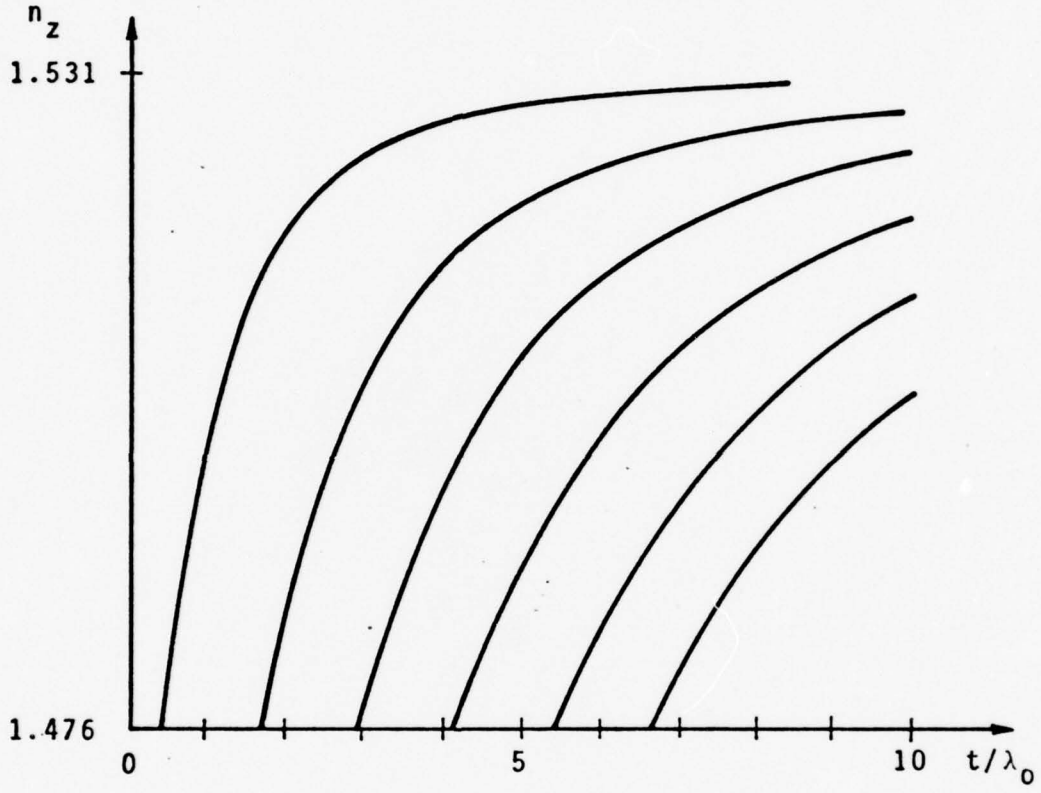

Figure 2-5. Typical solution curves to the eingenvalue equations for the planar waveguide for given values of n_1, n_2, n_3, as a function of core thickness (in units of wavelengths). It has been assumed $n_2 = 1.531$, $n_3 = 1.476$, and $n_1 = 1.000$.

3. RECTANGULAR FIBERS

3.1 Preparation of Rectangular Fibers

The rectangular fibers studied in the present work were pulled at the Ceramic Engineering Department of this University from a set of Schott optical glasses. Their commercial classification together with some of their thermal and optical properties according to the manufacturer's specifications are listed in Table 3-1.

The fabrication of rectangular fibers is a three step process. First a long ribbon of approximately 26 x 213 μm of core material is drawn from a 3 x 20 x 150 mm sheet of glass. Approximately 15 cm of this ribbon is placed between two similar sheets of cladding material and the resulting "sandwich" is heated to fuse the glass preform together. Experience has shown that the inner surfaces of the cladding sheets and the core should previously be carefully polished to avoid undesirable air bubbles at interfaces within the final fiber. This preform is then drawn into a long rectangular fiber by heating it in a cylindrical, vertical, hollow furnace above the glass softening point, and by pulling the heated preform end at a constant rate. If the temperature, the preform immersion rate and pulling speed are carefully adjusted lateral dimensions of the preform glasses are proportionally reduced to the final fiber dimensions.

The resultant long fiber ribbon is cut in a set of about 80 cm long fibers from which about ten are selected at random and classified for characterization. Finally a piece of typically 3 cm long

Commercial Classification	Refractive Index for λ = 0.8521 μm	Coefficient of Linear Thermal Expansion (-30° to 300°C) $\alpha \times 10^{-7}$/°C	Glass Transition Temperature (°C)
SSK2	1.61267	62/71	636
SK2	1.59847	60/70	654
SK6	1.60472	62/72	648
SK9	1.60483	60/70	638
SK11	1.55598	65/76	610
SK12	1.57487	64/75	633
SF7	1.62546	79/89	448

Table 3-1. Schott optical glasses used for the fabrication of rectangular fibers.

rectangular fiber with cleanly cut ends is removed from each of these ten fibers. The clean, 90° cut end is accomplished by producing a precisely defined flaw on the fiber's surface with a diamond knife while the tension and bending of the fiber are carefully controlled. Figure 3-1 is a photograph of the fiber cutting machine built in this department.[11] Once measured, the optical properties of these ten short fiber pieces were taken as typical of the pulled set.

Seven sets of fibers were thus prepared and studied for this work. Different glass combinations and/or geometries were chosen. Table 3-2 lists the glass combinations and resulting fiber parameters for each set. The NA values listed are calculated according to the selected bulk glasses index (see Table 3-1).

3.2 Near Field Measurements

Most of the information about the optical properties of a given fiber is contained in its cross sectional intensity distribution. A technique has been developed to actually measure these near field patterns. As will be shown, this method allowed experimental determination of two fiber parameters: core thickness (t) and numerical aperture (NA), defined in Section 2 as

$$NA = (n_2^2 - n_1^2)^{\frac{1}{2}} \qquad (3\text{-}1)$$

where n_2: refractive index of the core

n_1: refractive index of the cladding.

Figure 3-2 shows a schematic of the experimental setup. Figure 3-3 is a photograph of it. Light from a He-Ne, 2 mW laser source is coupled

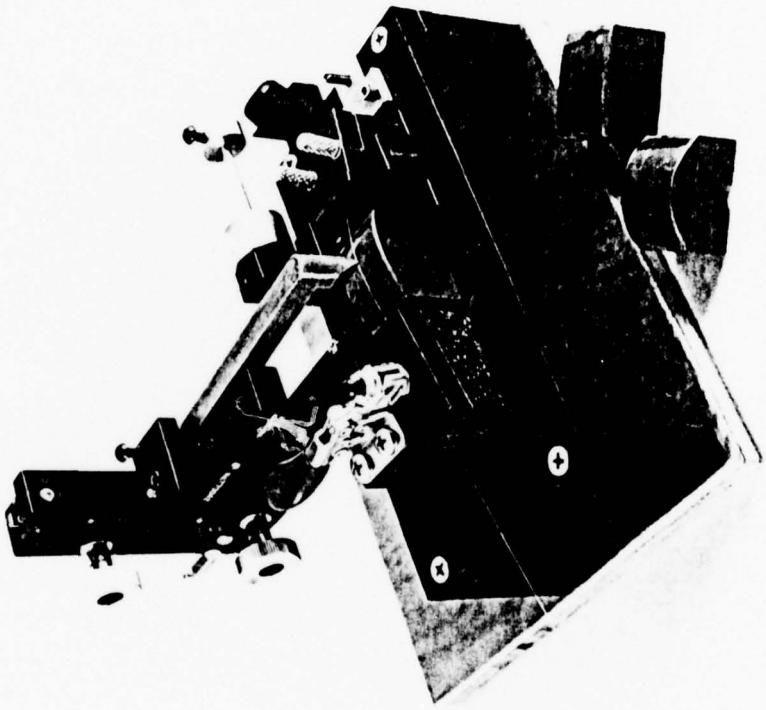

Figure 3-1. Fiber cutter built at the Electrical Engineering Department of the University of Washington.

Fiber Set #	Glass Combination	Numerical† Aperture	Typical Core Dimensions (μm)
1	SSK2 SK6	0.1599	1.6 x 28
2	SSK2 SK11	0.4238	2.0 x 26
3	SK9 SK2	0.1427	9.0 x 100
4	SK9 SK2	0.1427	2.9 x 21
5	SK9 SK12	0.3086	5.0 x 30
6	SK9 SK12	0.3086	3.1 x 27
7	SF7 SK12	0.4024	4.0 x 38

† Numerical aperture values are calculated according to the bulk glass indices listed in Table 3-1.

Table 3-2. Rectangular fiber sets fabricated and studied for this report.

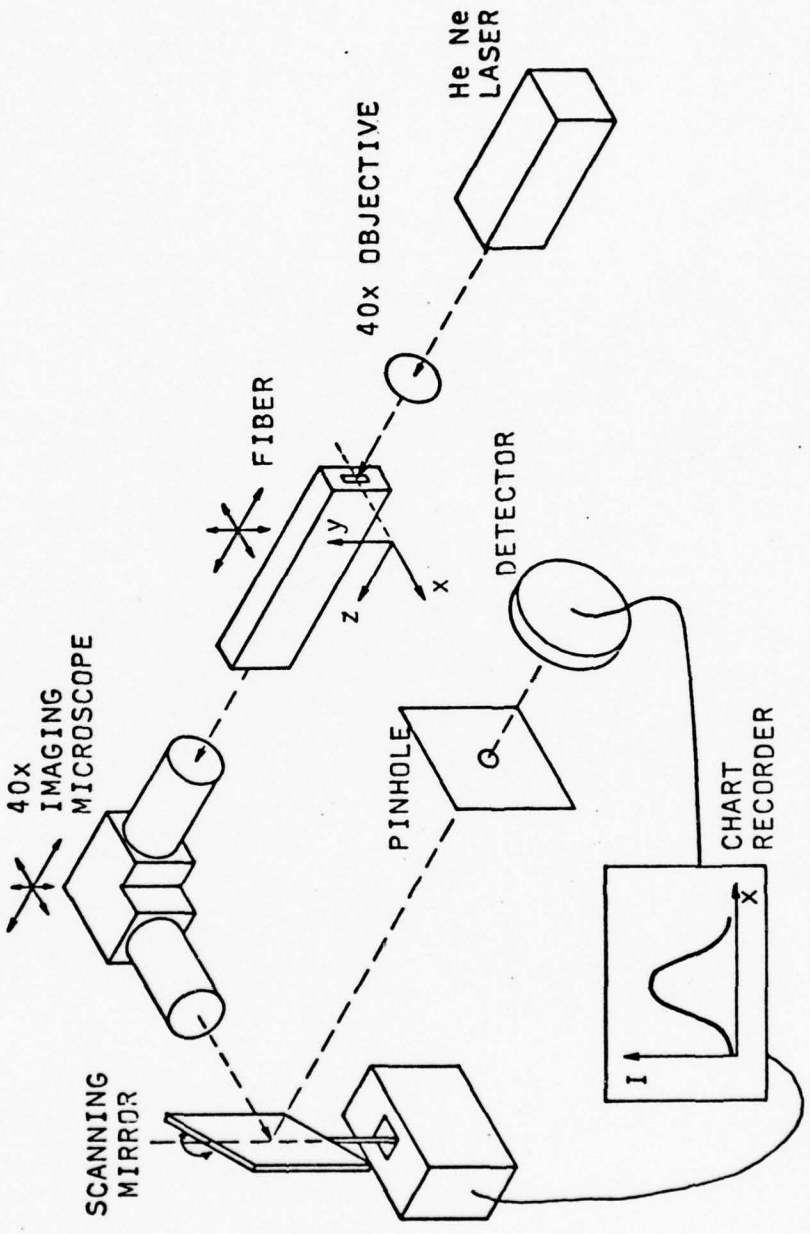

Figure 3-2. Diagram of the experimental set-up used to measure the near field intensity distributions of optical fibers.

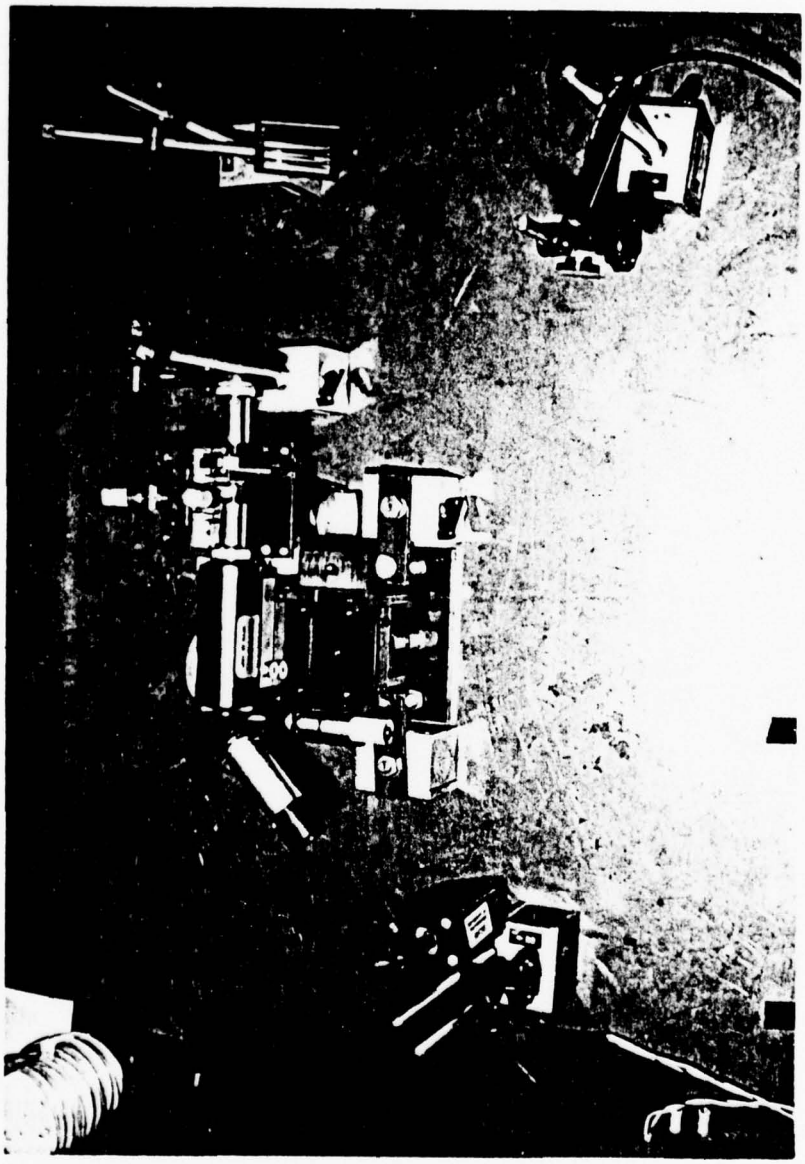

Figure 3-3. Photograph of the set-up shown in Figure 3-2.

into the core of a fiber by means of a 40x microscopic objective. Index matching oil (n = 1.6) was placed along 15 mm of the fiber surface to strip away unwanted cladding modes. A 40x microscope objective forms an image of the other end of the rectangular fiber on the detector mask via an oscillating mirror. A 0.51 mm diameter pin hole is placed immediately in front of the detector. Any desired magnification of the core image is easily obtained by adjusting the total microscope-mirror-detector distance. The mirror oscillates back and forth thus sweeping the core image across the detector pin hole in both directions. Its amplitude and frequency are adjustable. The angle of rotation is set to vary linearly with time, as the driving electrical current is of triangular shape. Finally, the mirror driver current and the detector output are fed into the x and y coordinates of a chart recorder. A plot of intensity versus distance (across the fiber end) is thus obtained. As will be seen in Section 4.4, for our purposes and geometry only the intensity distributions along the x axis are crucial. Figure 3-4 shows these near field intensity patterns for three typical fibers from different sets. Intensity scales are arbitrary. Sets number 1 and 2 yielded the highest measured coupling efficiencies (see Section 4). All other had efficiencies of the order of, or lower than set number 4. As may be noticed, one of the plots was repeated to check the consistency of the measurements. Distance calibration was performed by displacing the microscope with micro-positioner screws by a known amount and measuring the distance that

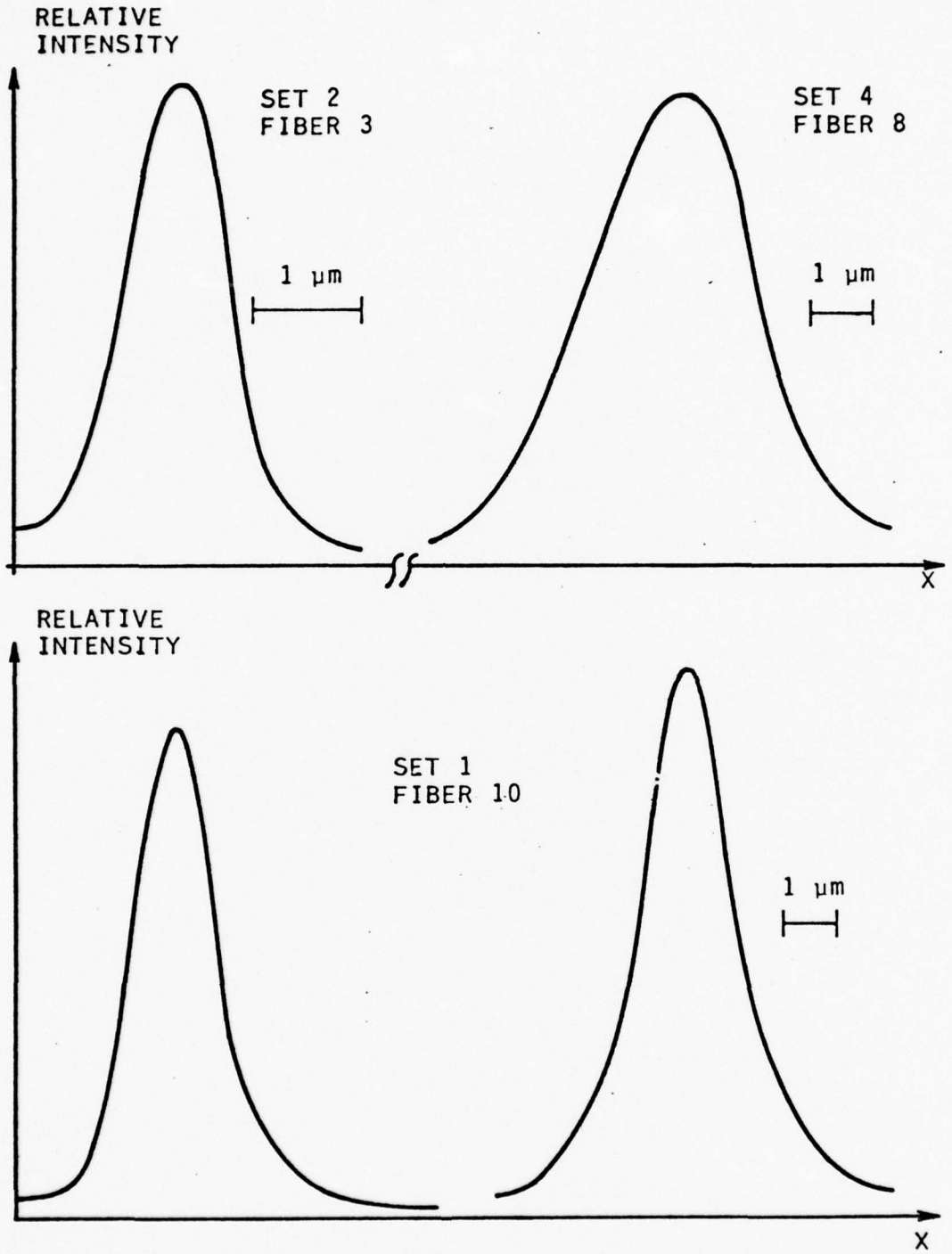

Figure 3-4. Near field intensity distributions versus x (see Fig. 3-2) for three rectangular fibers. Measurement was repeated for one fiber. The power scales are linear but arbitrary. Note that the distance scale (x) is different for different fibers.

the peak was displaced on the chart recorder. Figure 3-5 shows the calibration lines for each of the measured fibers.

Due to their high aspect ratio (width to thickness) we can approximately model these fibers as planar, symmetric waveguides (see Sections 4.3 and 4.4). According to the theory discussed in Section 2 field distributions for such single-mode guides should be of the form (see equations (2-23) and (2-31)):

$$\left.\begin{matrix} \text{TE} & E_{1y} \\ \text{TM} & H_{1y} \end{matrix}\right\} \quad \alpha \exp(-\alpha x), \text{ for } x \geq d$$

$$\left.\begin{matrix} \text{TE} & E_{2y} \\ \text{TM} & H_{2y} \end{matrix}\right\} \quad \alpha \cos(p_2 x), \text{ for } d \geq x \geq -d$$

$$\left.\begin{matrix} \text{TE} & E_{3y} \\ \text{TM} & H_{3y} \end{matrix}\right\} \quad \alpha \exp(\alpha x), \text{ for } -d \geq x \qquad (3\text{-}2)$$

where the origin of the x axis is taken as before at the center of the core region, and it is

$$\alpha = (\beta^2 - k_1^2)^{\frac{1}{2}} = k_o(n_z^2 - n_1^2)^{\frac{1}{2}}$$

$$p_2 = (k_2^2 - \beta^2)^{\frac{1}{2}} = k_o(n_2^2 - n_z^2)^{\frac{1}{2}} \qquad (3\text{-}3)$$

$$k_o = \frac{2\pi}{\lambda_o}$$

Since the intensity distribution is proportional to the square of the transverse fields, we have

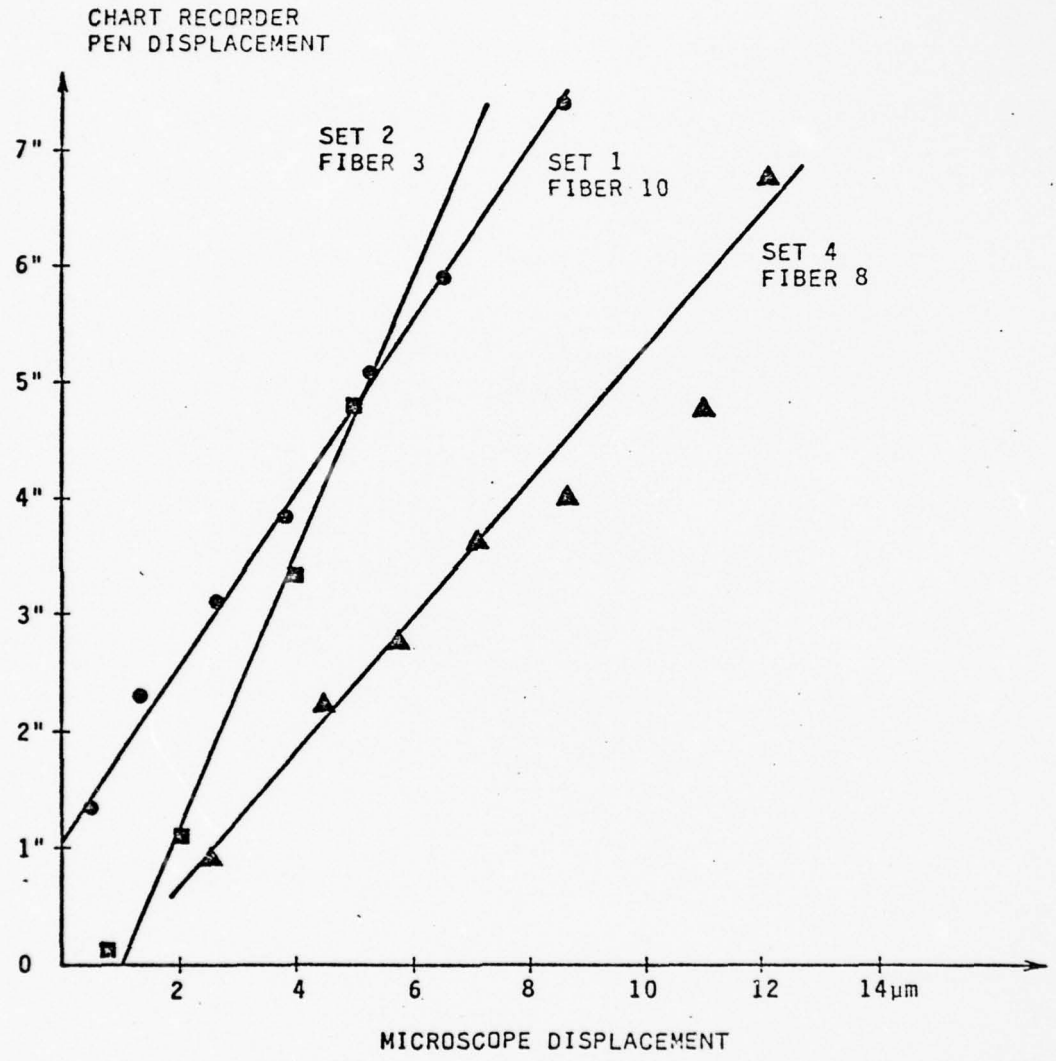

Figure 3-5. Distance calibration for each of the measured fibers.

$$I_1(x) \propto \exp(-2\alpha x), \text{ for } x \geq d$$

$$I_2(x) \propto \cos^2(p_2 x), \text{ for } d \geq x \geq -d$$

$$I_3(x) \propto \exp(2\alpha x), \text{ for } -d \geq x \qquad (3\text{-}4)$$

If the intensity distributions are plotted on a semilogarithmic scale, straight lines of slope 2α should then be obtained in the cladding regions. Figure 3-6 shows the semilogarithmic plots of the curves of Figure 3-4. The points at which each curve deviates from a straight line to form the peak define the boundaries of the core region. This method provides then a way of measuring the core thickness (t) with reasonable accuracy. It is only limited by the resolution of the imaging optics. In these measurements a 40x SWIFT objective of numerical aperture 0.65 was used. The error is then estimated to be on the order of 50%, which is reasonable since distances measured are on the order of two or three wavelengths.

The determination of fiber numerical apertures is somewhat more involved. From equation (3-3)

$$NA = \left[\left(\frac{p_2}{k_o}\right)^2 + \left(\frac{\alpha}{k_o}\right)^2\right]^{\frac{1}{2}} = \frac{\lambda_o}{2\pi}\left(p_2^2 + \alpha^2\right)^{\frac{1}{2}} \qquad (3\text{-}5)$$

We can determine p_2 and α for each fiber from the corresponding semilogarithmic plot. Indeed, from equation (3-4) it is

$$\frac{I_2(d)}{I_2(o)} = \cos^2(p_2 d)$$

So

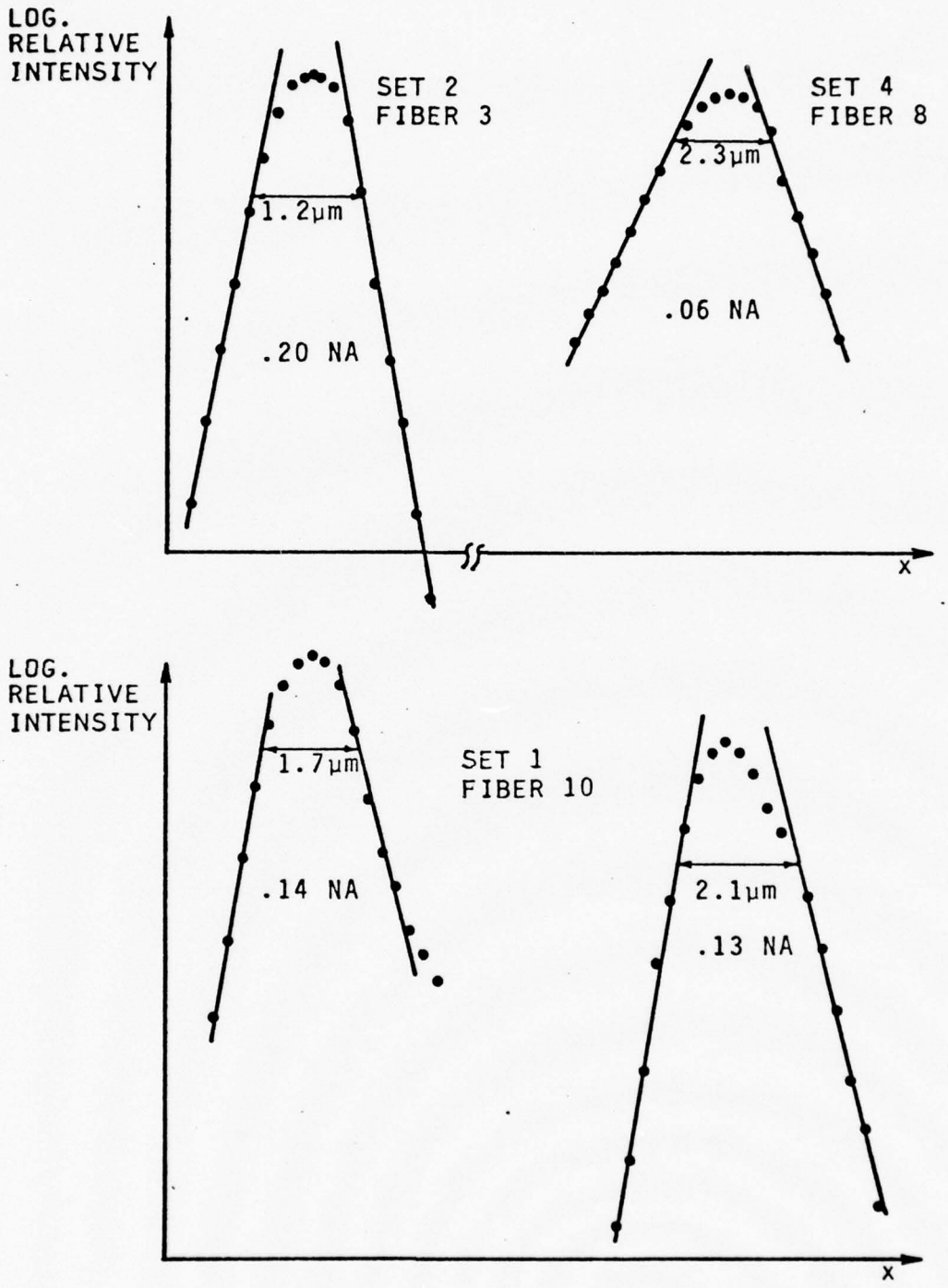

Figure 3-6. Semilogarithmic plots of the near field intensity distributions of Figure 3-4. The core dimensions and calculated NA values are shown for each fiber.

$$p_2 = \frac{1}{d} \arccos\left[\left(\frac{I_2(d)}{I_2(o)}\right)^{\frac{1}{2}}\right] \qquad (3\text{-}6)$$

The ratio of intensities at the cladding/core boundary $I_2(d)$, to the peak value $I_2(o)$ can easily be read off the graph. On the other hand α can be obtained from the slope of the straight lines representing the intensity in the cladding. From equation (3-4) it is

$$\log[I_1(x)] = \text{constant} - mx$$

where

$$\left| \frac{\log I_1(x_2) - \log I_1(x_1)}{x_2 - x_1} \right| = m = 2\alpha \log e$$

so then

$$\alpha = \frac{1}{2 \log e} \left| \frac{\log[I_1(x_2)/I_1(x_1)]}{x_2 - x_1} \right| \qquad (3\text{-}7)$$

From equations (3-5), (3-6) and (3-7) we can then determine the NA of the tested fiber from the plots. Table 3-3 lists the measured core thicknesses and NA values for the three fibers tested and the repeated measurement. It should be pointed out that even though a 50% error has been mentioned, straight line fits to the corresponding data points are fairly accurate. Furthermore NA values do not differ more than 20% when taken from both lines on either side of each curve, or between the two measurements of the same fiber. Also listed in the table for comparison are the NA values calculated according to the manufacturer's bulk index data for the chosen glasses. It is apparent that on heating and pulling the fibers a drastic reduction of the difference in index

Fiber Set #	Fiber #	Numerical Apertures		Core Thickness (μm)
		Nominal†	Measured	
1	10	0.1599	0.137	1.7
1	10	0.1599	0.135	2.1
2	3	0.4238	0.205	1.2
4	8	0.1427	0.058	2.3

† Nominal values of NA are calculated according to the manufacturer's bulk index data for the chosen glasses (see Tables 3-1 and 2).

Table 3-3. Measured parameters for typical samples of the three fiber sets which yielded the highest laser/fiber coupling efficiencies (see Section 4.5).

of refraction of the glasses takes place. Given the dimensions involved it is reasonable to assume that most of this alteration occurs to the core material. At present two possible explanations have been proposed. There is the possibility of interdiffusion between both glasses during the heating processes; or perhaps even more probable is the possibility of strain at the core/cladding interface during the cooling process due to different thermal expansion coefficients for each glass. Further research in this area would be needed to achieve better control over the final values of the fiber parameters.

Another optical property of interest is the power loss per unit length due to scattering and absorption of the propagating wave. A discussion of this parameter will be postponed to Section 4.5.

4. THE SOURCE/FIBER COUPLING PROBLEM

4.1 Coupling Light Between Two Waveguides

Even though many different coupling schemes have been studied, they can be classified as one of two basic methods: i) coupling by direct excitation, and ii) evanescent field coupling. The direct excitation method consists of bringing the two component waveguides together end to end, aligning their optical axes. This approach clearly requires that a clean, sharp 90° cut be performed at the end of each waveguide. The coupling efficiency then depends on matching the field patterns of both guides. This in turn imposes serious alignment restrictions. Due to the typical dimensions of components, misalignments of the optical axes by just a few microns is usually sufficient, even in multimode fiber systems, to reduce coupling efficiencies by at least a factor of two. This method nevertheless has yielded better results in fiber/fiber, source/fiber coupling; and in thin-film/thin-film and fiber/thin-film coupling when the two waveguides have vastly different refractive indices.

The evanescent field coupling method consists of superimposing both waveguides as shown in Figure 4-1, so that the evanescent tails of their field distributions (see Section 2) may overlap. If the propagation constants β (or equivalently the phase velocities along the z direction) are matched, a tunneling effect takes place across the gap between guides and power is transferred from one guide to the other. Alignment tolerances in this case are far less critical

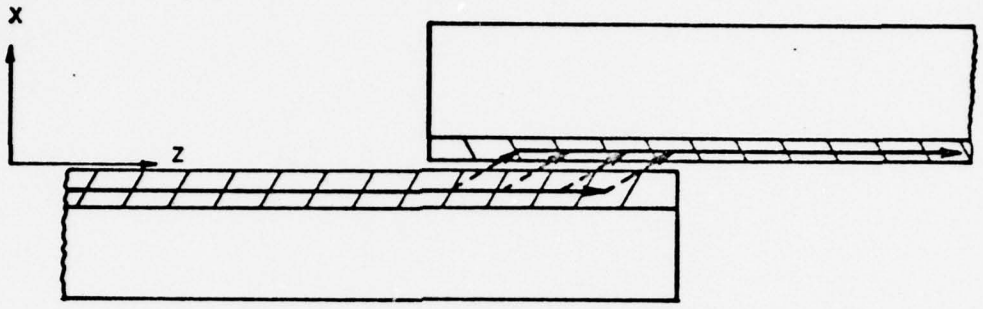

Figure 4-1. Evanescent field coupling between two thin-film waveguides.

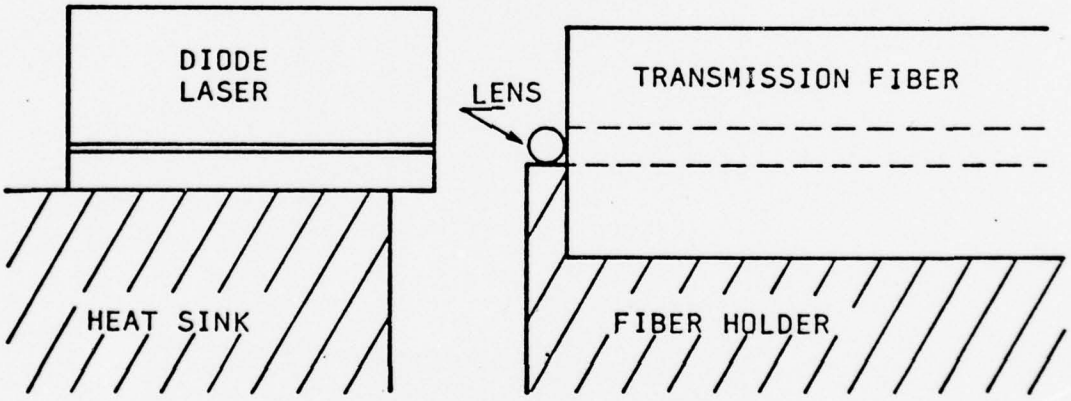

Figure 4-2. Proposed laser/fiber coupler using a cylindrical lens.[7]

since power transfer takes place over a distance of a hundred to a few thousand wavelengths. This approach also enables needed mechanical rigidity. As stated, this method is preferred in thin-film/thin-film and fiber/thin-film coupling but only when both guides have similar refractive indices. In the fiber/thin-film case however, the core must be exposed by uncladding the fiber to allow overlapping of the evanescent fields. A further difficulty results from the geometrical mismatch between the planar thin-film waveguide and the cylindrical fiber core. The proposed rectangular-to-round transition fiber, but with an externally mounted core in this case, could also here be the solution.

4.2 Source/Fiber Coupling. Review of Published Results

As their name indicates DH laser sources of "stripe" geometry have their active layer "buried" or surrounded by doped semiconductor material. Furthermore there are no known transparent materials in the visible or near infrared regions with index of refraction high enough to match that of the GaAlAs laser. Evanescent field coupling in this case then is not possible.

Different direct excitation source/fiber coupling schemes have been reported. L. G. Cohen[3] obtained coupling efficiencies of about 2% to 14% between two DH lasers and two (round) single-mode fibers, with a single measurement of 25%. We should note however that his measured laser output had dimensions of 1 x 3 μm. It should also be mentioned that he subtracted from his reference the fluorescent light

power which, according to the author, amounted to about 46% of the total laser output.

L. P. Boivin[4] has proposed a hybrid laser-thin-film waveguide-round fiber structure. His best over all measured efficiencies into a 10 μm diameter (multimode) fiber core were of order 10%.

Several microlenses have been suggested in order to collimate the strongly divergent laser beam along the x direction or to reshape it.[5-7] E. Weidel reported a coupling efficiency of 40% between a DH laser and a monomode fiber on which a hemicylindrical lens, with its axis along the plane of the laser junction, had been etched at the input end by a photolithographic technique.[6] The author mentions however that the width at half power along the plane of the junction for the fiber and laser used were 3.1 μm and 13 μm respectively. In a subsequent paper[7] E. Weidel reports experimental coupling efficiencies of up to 103% and of an average of 60% to 70% between a monomode fiber with a cylindrical lens in front and a DH laser. A schematic of the set-up is shown on Figure 4-2. The cylindrical lens is made with another fiber of 10 μm diameter and approximately the same refractive index of the transmission fiber. The higher than 100% efficiency is explained on the basis that the plane face of the transmission fiber and the laser mirror set up a new Fabry-Perot resonant cavity as they are brought close to each other. This, according to the author, changes the effective reflectivity of the laser mirror. Even though this is a known effect, it is difficult to justify such an increase

of the laser output. Laser mirrors have an optimum value for the reflectivity below and above which power output decreases.[12] Furthermore the cylindrical lens in front of the transmission fiber would set up in any case a highly lossy Fabry-Perot cavity due to reflections on the convex shaped cylindrical surface.[13] We should also add that the author subtracts 26% of the total laser output power used as reference as due to fluorescent light.

In these papers cladding modes have been stripped away by allowing the tested fiber to be in contact with index matching oil along a few centimeters before measuring the light output at the fiber end. Our experience has shown this method to be not satisfactory since much light still is observed in the cladding at the output end. Finally, by placing the axis of the cylindrical lens along the plane of the junction (yz), the problem of field pattern mismatch along this direction is still unresolved. Of all the above works only Boivin's paper addresses this question.

It is in view of these facts that we still consider a 25% efficiency to be a reasonable estimate of the maximum attainable value unless the fields mismatch along the plane of the junction is considered. In fact the best source/single-mode (round) fiber coupling efficiencies observed at the Naval Ocean Systems Center are of the order of 6%.

4.3 The Laser Source

Figure 4-3 shows a schematic of a typical DH laser. The stripe at the center of the active layer has a rectangular cross section with typical dimensions of about 0.2 x 11 μm. The laser chip is usually soldered to a copper mount for mechanical rigidity and heat sinking purposes. Current is injected from the top through a thin soldered wire.

As has been stated the elliptical output beam has typical dimensions of about 1 x 13 μm. As the light leaves the mirror surface, it suffers strong diffraction due to the small size of the aperture. In many studies then, even though the laser is a symmetric, almost planar guiding structure as discussed in Section 2, to a good approximation the outcoming beam is considered to be Gaussian. Furthermore, since the dimensions of the beam along each direction differ by at least an order of magnitude, variations along x and y are usually considered independent. The original two dimensional problem is thus divided into two one dimensional ones. Using the Gaussian beam model and the typical laser output dimensions, it is easy to obtain an order of magnitude estimate of the beam parameters. Taking the half widths at minimum beam waist at the mirror surface to be W_{ox} = 0.5 μm and W_{oy} = 6.5 μm, λ_o = 0.85 μm; the Rayleigh range[14] (Z_R) along each direction results:

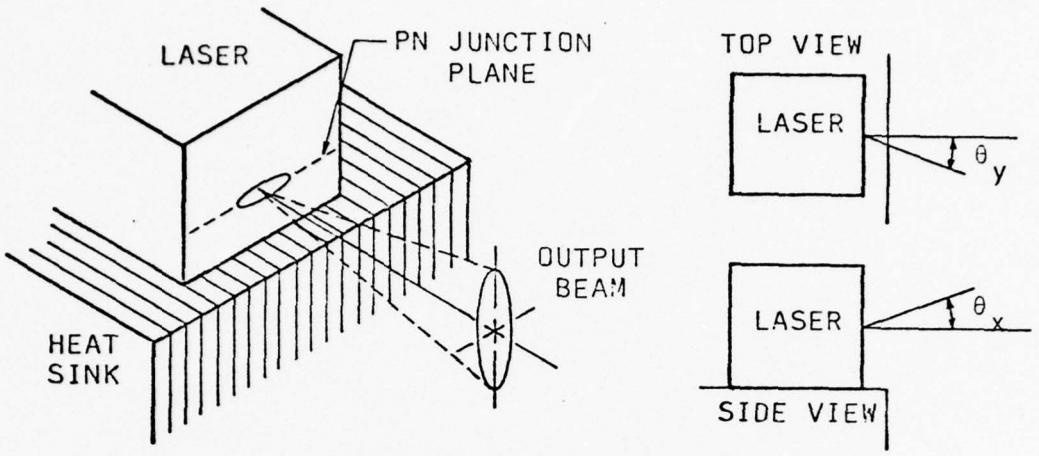

Figure 4-3. Schematic of a typical DH injection laser.

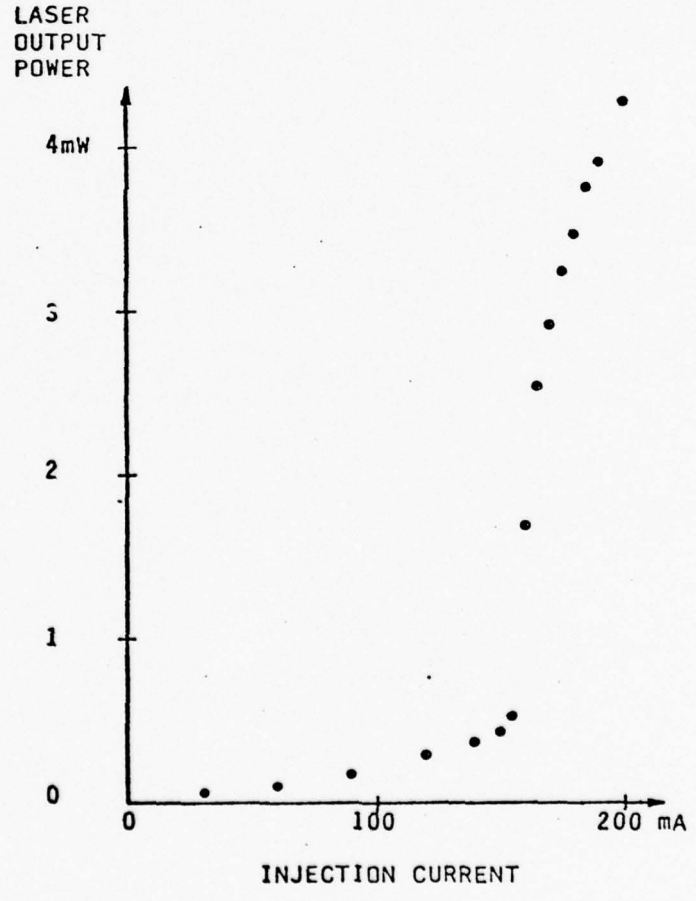

Figure 4-4. RCA DH laser #866, response curve.

$$Z_{RX} = \frac{\pi W_{ox}^2}{\lambda_o} \cong 0.9 \ \mu m$$

$$Z_{RY} = \frac{\pi W_{oy}^2}{\lambda_o} \cong 156 \ \mu m \qquad (4\text{-}1)$$

The half angle of divergence of the beam is

$$\theta_{ox} = \text{arc tan}\left(\frac{\lambda_o}{\pi W_{ox}}\right) \cong 28°$$

$$\theta_{oy} = \text{arc tan}\left(\frac{\lambda_o}{\pi W_{oy}}\right) \cong 2° \qquad (4\text{-}2)$$

It is now clear why several microlenses have been designed to collimate the strongly divergent beam along the x direction, for a fiber placed just a few microns ($> Z_{RX}$) away from the laser. It is also clear that in order to match the field distribution of the laser output before strong distortion and expansion of the beam takes place, a rectangular fiber must be placed a distance of the order of or less than Z_{RX} from the laser. As will be discussed, this demands extremely fine control over displacements, as well as good stability of the mechanical set up.

For our studies we used an RCA DH injection laser. Figure 4-4 shows its response curve: optical output power versus input injection current. Figures 4-5.a and b show its measured far field intensity distributions along the x and y directions respectively. These measurements were done by placing a detector with a 0.51 mm diameter pin hole, 17.6 mm ($>> Z_{RY} >> Z_{RX}$) away from the laser. The latter was then displaced along the xy plane with micropositioning screws.

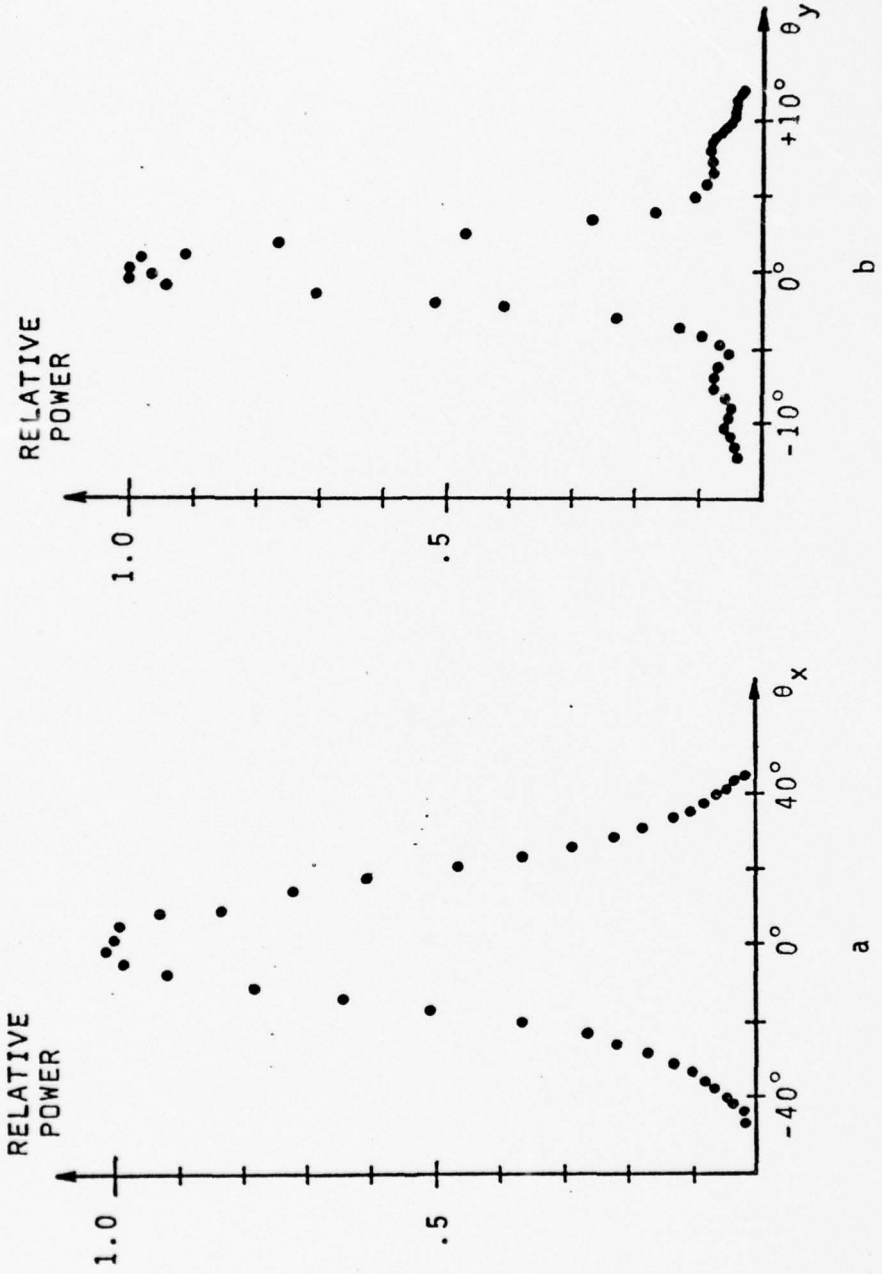

Figure 4-5. Measured far field intensity distributions for the RCA DH laser #866.
a. Along the xz plane perpendicular to the junction.
b. Along the yz plane of the junction.

The angles shown in the figures refer to the angle subtended by the optical axis of the laser and the pin hole, as seen from the source. Suitable corrections were made on the original data to account for:

i) Laser-pin hole distance change as the laser was moved on the xy plane.

ii) Change in the solid angle subtended by the pin hole (always parallel to the xy plane) as seen from the laser.

As expected from our previous estimations the far field pattern along the xz plane perpendicular to the junction (Figure 4-5.a) is much broader than the corresponding pattern along the yz plane of the junction (Figure 4-5.b). Much stronger diffraction of the beam occurs along the first plane. Positive angles in both cases refer to angles generated from the optical axis towards the +x and +y directions respectively. It is interesting to notice a slight asymmetry of both curves.

If we assume both plots to be approximately Gaussian, we may estimate the beam dimensions at the mirror of our particular laser. Indeed, since these plots represent intensity rather than field distributions, taking the half divergence angle (θ) at $(1/e)^2$ of the peak value, we can use again equation (4-2) to obtain now the half width at minimum beam waist:

$$W_{ox} = \frac{\lambda_o}{\pi \tan \theta_{ox}} \cong \frac{0.85\ \mu m}{\pi \tan(30.2°)} \cong 0.46\ \mu m$$

$$W_{oy} = \frac{\lambda_o}{\pi \tan \theta_{oy}} \cong \frac{0.85\ \mu m}{\pi \tan(4.1°)} \cong 3.8\ \mu m \qquad (4\text{-}3)$$

As expected the beam thickness ($2W_{ox}$) is of the order of 1 μm. It is not surprising however to obtain a beam width ($2W_{oy}$) smaller than the typical value. As is often the case, the Gaussian beam approximation is not satisfactory along the plane of the junction. In fact a closer look at Figure 4-5.b reveals the typical side lobe structure of the far field intensity distribution for a rectangular aperture. This pattern was also observed with an infrared viewer on the pin hole screen in front of the detector. The intensity distribution in this case is given by[15]

$$I_y(y) \propto \frac{\sin^2(\frac{k_o\, y\, W_{oy}}{z})}{(\frac{k_o\, y\, W_{oy}}{z})^2} \qquad (4\text{-}4)$$

where it is

$$\frac{y}{z} = \tan(\theta_y)$$

The first null of the distribution then occurs for

$$k_o\, W_{oy}\, \tan(\theta_{1y}) = \pi \qquad (4\text{-}5)$$

or equivalently for

$$W_{oy} = \frac{\lambda_o}{2\, \tan(\theta_{1y})} \cong \frac{0.85\ \mu m}{2\, \tan(5°)} \cong 4.9\ \mu m$$

the estimated width of our laser output is then of about 10 μm.

4.4 The Source/Rectangular Fiber Coupling Problem

As has been mentioned, good coupling efficiency by direct excitation depends on matching the field patterns of both component waveguides

as they are brought together along their optical axis. It has been pointed out[16] that due to the laser's strongly rectangular output, most of its radiation can be coupled into a similar rectangular waveguide if the numerical aperture (NA) of the latter (see Sections 2 and 3) exceeds at least the angle of divergence of the source along the plane of the junction (θ_{oy}). This is intuitively clear. Given the relationship derived in Section 2 between NA and far field divergence angle for a planar waveguide, namely

$$NA = \sin (r) \tag{4-6}$$

we are simply requiring then that the fiber half angle of divergence exceeds that of the laser along the plane of the junction:

$$\sin (r) > \sin (\theta_{oy}) \sim \theta_{oy} \tag{4-7}$$

The laser/fiber coupling coefficient (η) then depends only on the overlap integral of the field distributions along the x axis. Rigorously it is

$$\eta = \frac{\int_{-\infty}^{\infty} f_L(x) \cdot f_F(x)\, dx}{\left(\int_{-\infty}^{\infty} f_L^{\,2}(x)\, dx\right)^{\frac{1}{2}} \left(\int_{-\infty}^{\infty} f_F^{\,2}(x)\, dx\right)^{\frac{1}{2}}} \tag{4-8}$$

where

$f_{\substack{L \\ F}}(x)$: field distribution of the $\binom{\text{laser}}{\text{fiber}}$ along the x axis

Theoretical calculations of η have been carried out[16-18] for these geometries assuming $f_L(x)$ to be a Gaussian distribution in some cases,

and a typical cosine function with exponential tails in others. For the fiber $f_F(x)$ is usually of the latter form, as derived in Section 2. Optimum coupling efficiencies range between 65% and 98% depending on the modeling assumptions and waveguide parameters. As it has been stated however, alignment tolerances are critical. Displacements of a few microns along the x direction are enough to offset both distributions, thus reducing η by at least a factor of two.

At this point it may seem that the experimental problem reduces to obtaining a fiber with the same indices and geometry of the laser. This is not the case since:

i) As stated there are no transparent materials with such high refractive indices.

ii) In order to later obtain high transition fiber/round fiber coupling efficiency their NA and geometries must be matched. Obtaining a rectangular fiber with the same NA as the laser, even though possible, would not be desirable since much loss would occur later in the transition/round coupling due again to field mismatch at the interface.

Commercially available single-mode, round transmission fibers have NA values of approximately 0.16 ($r \sim 9°$) and core diameters of about 3 to 6 μm. Our final aim is to optimize overall laser-transition-transmission fiber efficiency. In the following section we concentrated on the study of the source/waveguide efficiency using rectangular fibers with NA values close to the 0.16 value of regular transmission fibers.

4.5 Coupling Efficiency Measurements

Conceptually coupling efficiency measurements are simpler than those described in previous sections. Experimentally however they are much more difficult. Figure 4-6 shows a schematic of the set up. Figure 4-7 is an actual picture of it. Optical power from the laser is directly coupled into a short section of a rectangular fiber. A microscope (40x objective) is focused onto the fiber output and the image is projected and amplified onto the detector. A small, adjustable, rectangular screen is used immediately in front of the detector to block the fiber core image. The detector signal is amplified and fed into a digital voltmeter (DVM). The laser cw output is fixed by adjusting the value of the injection current. By subtracting then the power read from the DVM when the screen is adjusted to block the core image from the total power (core plus cladding), read without the screen, a measurement of the power transmitted through the core is obtained. Core image blocking and other image positioning adjustments are observed through an infrared viewer. The ratio of the measured core power value to the laser output for a given injection current gives us the desired coupling efficiency value for the fiber.

Table 4-1 contains a summary of coupling results. Typical measured coupling efficiency values for each set are listed under column n_1. The fiber number is given in each case for future reference in the event of further research. Sets number 1 and 2 yielded the highest efficiencies. More than one value has then been listed to show data

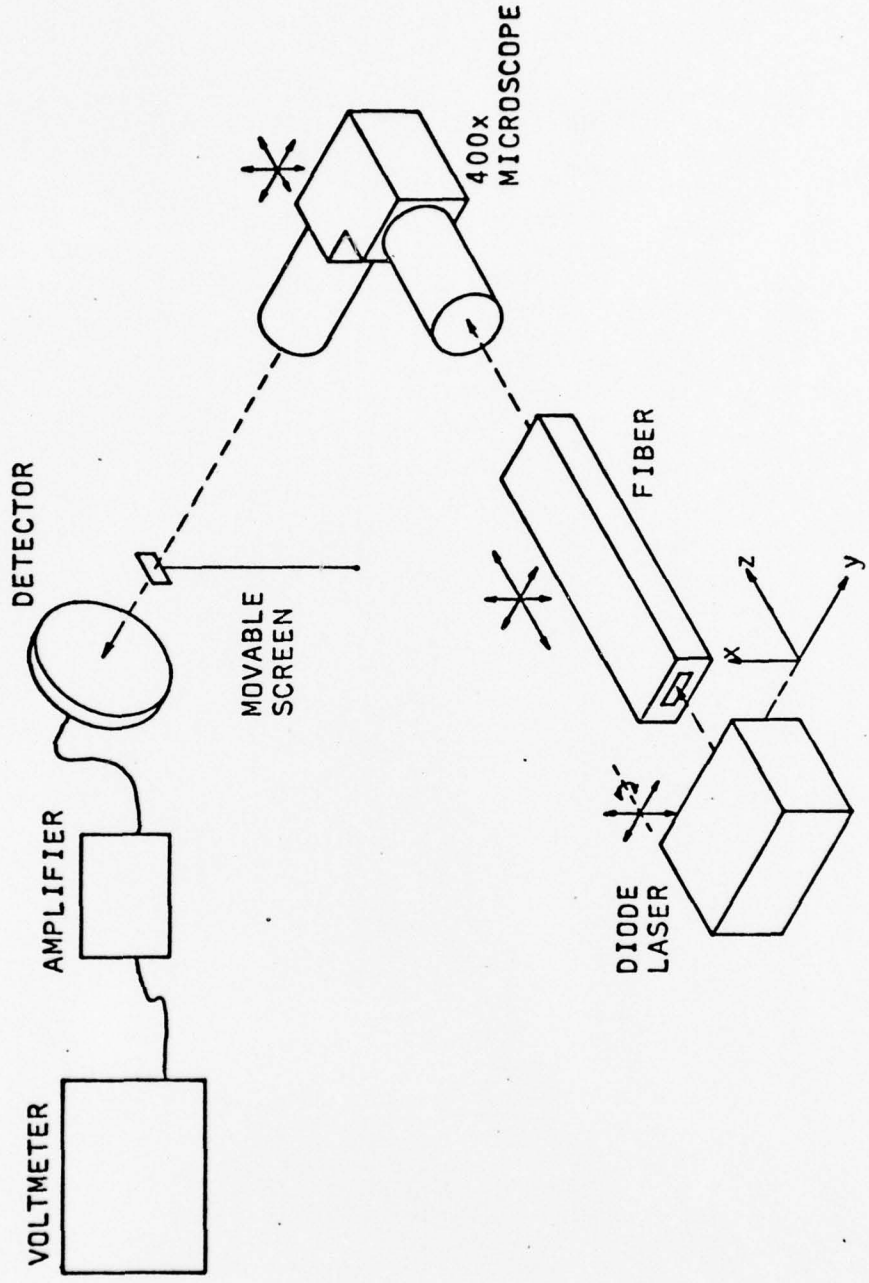

Figure 4-6. Diagram of the experimental set-up for measuring laser/ rectangular fiber coupling efficiency.

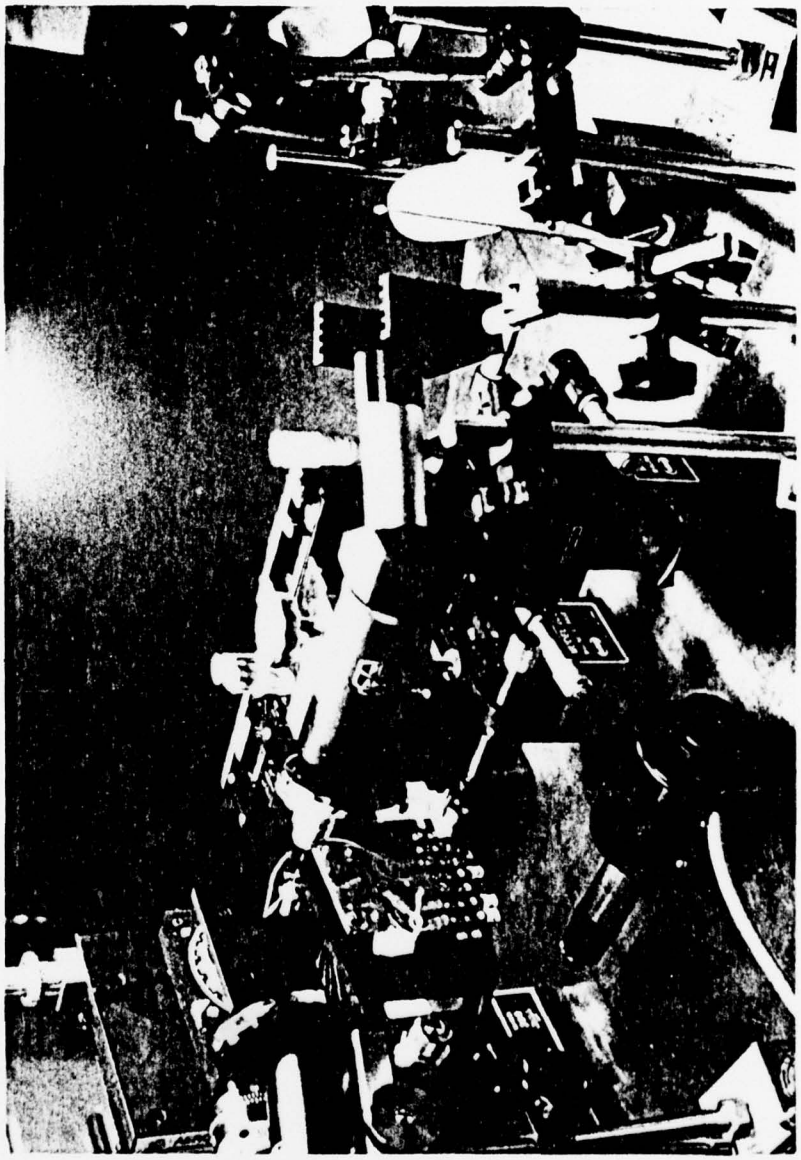

Figure 4-7. Photograph of the set-up shown in Figure 4-6.

Fiber Set #	Numerical Aperture†		Fiber #	Core Dimensions (μm)	Coupling Efficiency††		
	Nominal	Measured			η_1%	η_2%	η_3%
1	0.1599		4	2.0 x 24	9.6	20.0	28.0
		0.14	10	1.7 x 34	10.0	23.0	33.0
2	0.4238	0.20	3	1.2 x 16	14.5	24.0	34.0
			14	2.8 x 31	7.4	15.0	21.0
			16	2.8 x 22	14.0	32.0	46.0
			18	2.5 x 32	25.0	50.0	71.0
3	0.1427		4	10.0 x 88	4.4	10.0	14.0
4	0.1427	0.06	8	2.3 x 34	4.6	10.0	14.0
5	0.3086		5	5.5 x 34	2.7	5.0	7.0
6	0.3086		2	3.2 x 27	2.0	4.0	6.0
7	0.4024		all	4.0 x 38	0.0	0.0	0.0

† See Table 3-3.

†† η_1: uncorrected measurements

η_2: corrected values accounting for transmission losses through the sample fiber.

η_3: values after correcting for both transmission losses and fluorescent power.

Table 4-1. Summary of laser/rectangular fiber coupling results.

variance. Fiber #3 in the second set is a transition fiber. Its efficiency nevertheless is of order 14%, a typical value for this set. Fiber #18 yielded the highest directly measured efficiency to date in our laboratory. Fiber parameters are also listed in this table for analysis and comparison. As described in Section 3.2 fiber NA values were measured for the three sets with highest coupling efficiencies. Measured core dimensions are also included in each case. Core thicknesses however, except for those measured with the technique described in Section 3.2, have an error of ±1 μm.

Coupling efficiency results discussed so far do not include any corrections. In order to account for the possible power loss as the light travels through the rectangular fiber core, a longer piece of fiber from set #2 (corresponding to fiber #18) was prepared with cleanly cut ends and placed in lieu of the short fibers in the set-up. Core power output was measured as a function of fiber length by succesively shortening the fiber at the output end. Care was taken in each measurement to optimize laser/fiber coupling. Figure 4-8 shows the resulting plot. The power scale is in decibels (dB), but otherwise arbitrary. A loss of 1 dB/cm with approximately a 10% error is obtained. The transmission loss for each sample fiber can now be calculated according to its length. For set #2 typical 32% and a maximum coupling efficiency of 50% are thus obtained. A 1 dB/cm loss corresponds to 10^5 dB/km. Such a large figure is naturally believed to be due to the fiber fabrication process, i.e. scattering due to air bubbles,

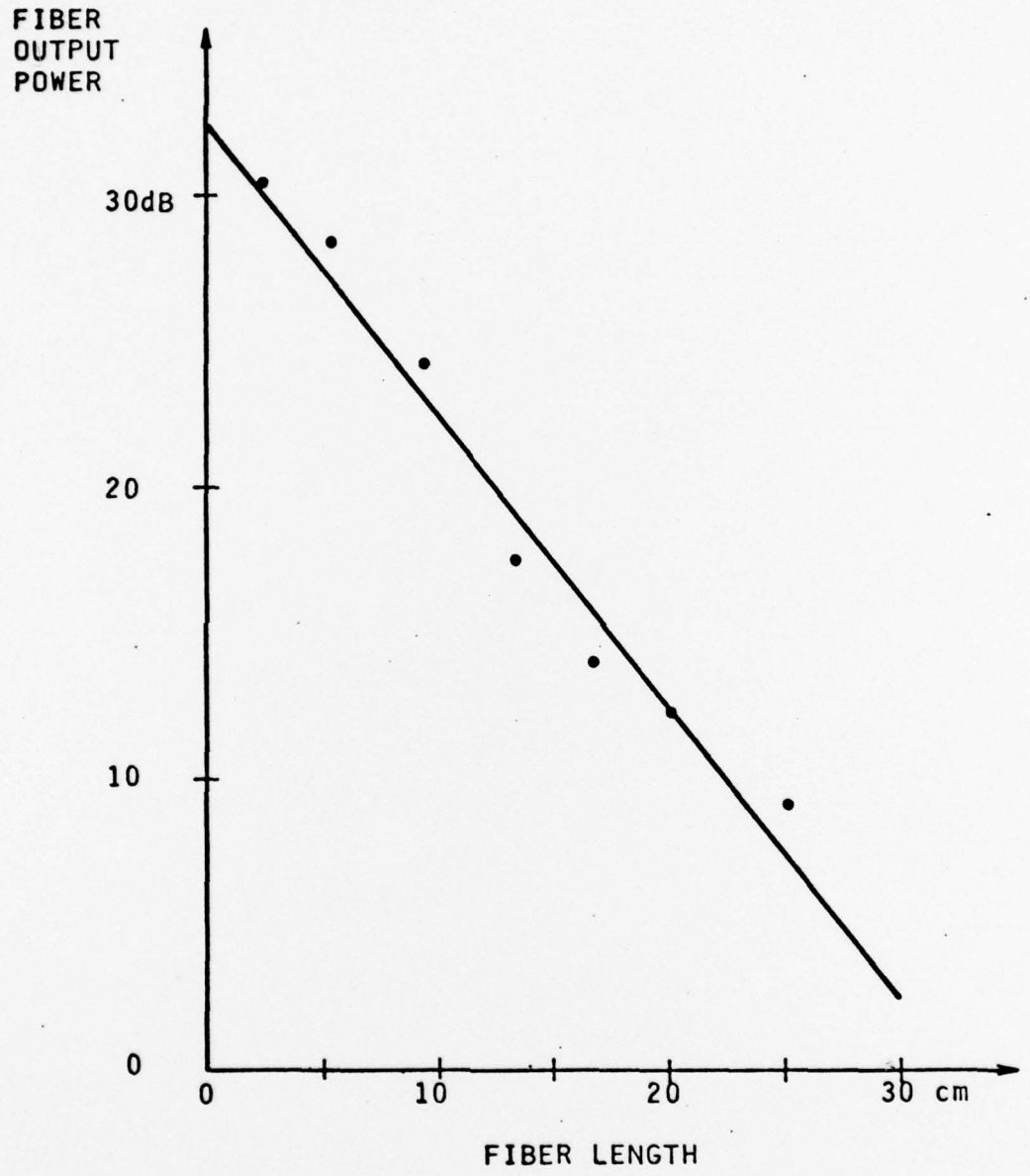

Figure 4-8. Fiber core power output as a function of fiber length.

impurities and imperfections especially at the core/cladding interface, rather than to bulk absorption by the glass. Considering a 1 dB/cm loss, column η_2 in Table 4-1 represents the corrected coupling efficiency accounting for the length of each sample fiber.

In order to compare these results with those reported in other publications an additional correction factor for fluorescent power must also be included. To do this a plot of output power versus laser injection current must be obtained for both the laser/fiber system and for the source itself (see Figure 4-4). The prethreshold curve is then linearly extrapolated in both plots through threshold to the operating current, neglecting the lasing portion of the curve. The extrapolated power value at the operating current (P_F) is considered as due to fluorescent or incoherent radiation, and is subtracted in each case from the total output power (P_0). Coupling efficiency is thus obtained as

$$\eta = \frac{P_{10} - P_{1F}}{P_{20} - P_{2F}} \qquad (4\text{-}9)$$

where P_1: power output from the fiber core

P_2: power output from the laser

This correction was performed for set #2; a set having a high expected P_{1F} value, obtaining typical 20% and maximum 36% efficiencies from raw data. This represents an increase of about 1.4 over the values listed under column η_1 in Table 4-1. This is not surprising since we should expect the laser radiation to couple more efficiently into the fiber.

Applying now the correction for transmission losses on these efficiency figures, typical 46% and maximum 71% efficiencies are obtained. Column η_3 in the table represents coupling efficiency results after having corrected the original data for both fluorescence and transmission losses. We should note however that this correction for fluorescent power is a way of idealizing or normalizing for one parameter of the laser output. In present day technology all injection DH lasers have a similar fluorescent power component. Even though coupling efficiency results are in general improved by this correction, they do not represent then actual efficiencies.

Figure 4-9 shows raw (η_1) and corrected (η_2) efficiencies versus NA for fibers with a 2 μm core thickness. Figure 4-10 is a plot of output power (or efficiency) versus laser/fiber distance (d). The zero of the distance scale is arbitrary however and does not represent zero laser/fiber distance. Peaks appear as a result of the Fabry-Perot cavity formed by the laser mirror and the fiber end. The measured distance between peaks is about half a wavelength as would be expected. The fast overall decrease of the power for increasing distances clearly shows how critical positioning tolerances are. In fact this plot was extremely difficult to obtain even with differential screw micropositioners because of optical table vibrations. The following section briefly summarizes experimental considerations.

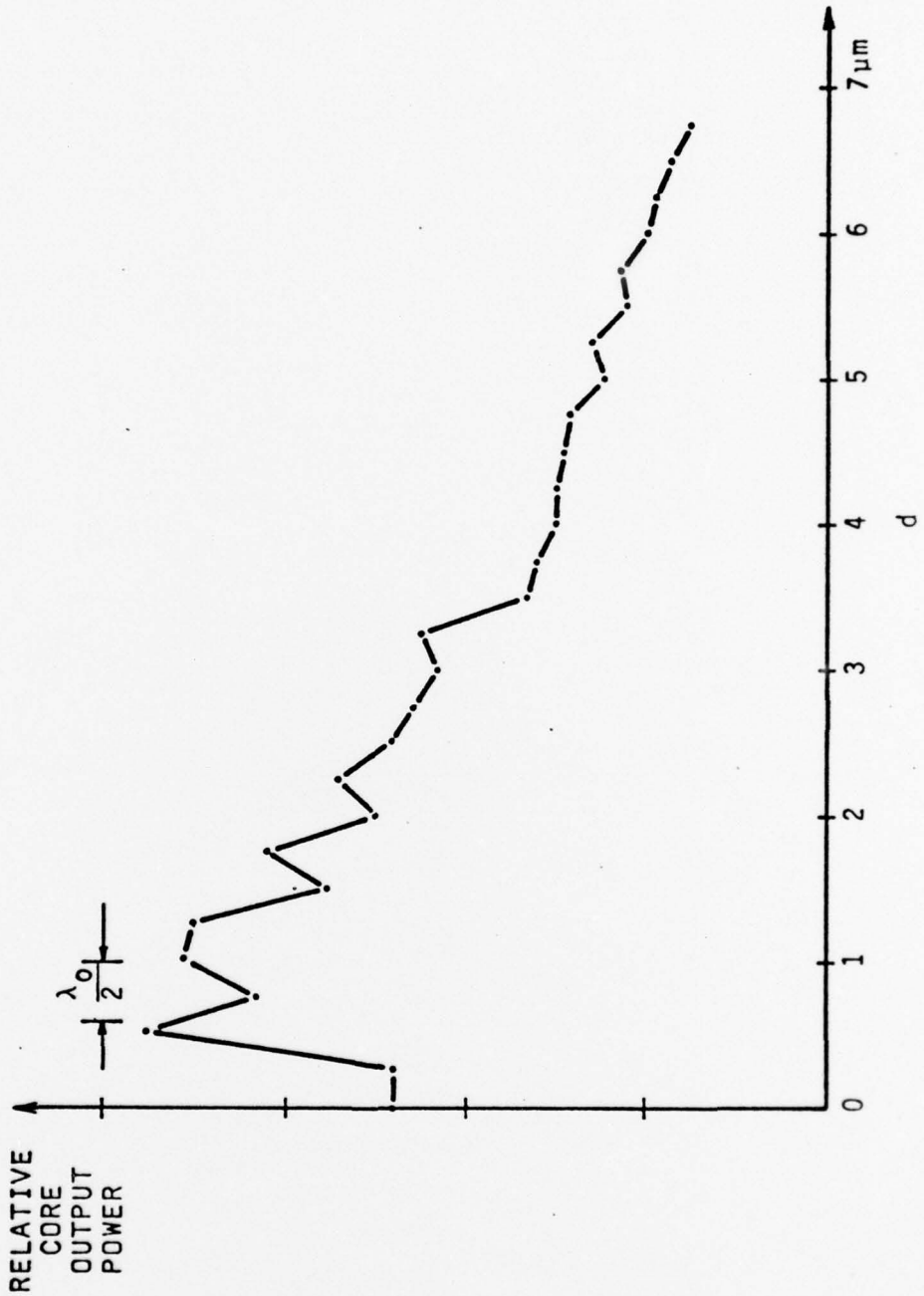

Figure 4-10. Fiber core output power as a function of laser/fiber distance (d). The transition fiber in Table 4-1 was used for this test. The zero distance reference is arbitrary.

4.6 Experimental Difficulties

As previously stated, experimental difficulties are far more serious than the initial description might suggest. A brief discussion of the principal problems together with some suggestions for future improvement should prove useful in case of further research:

i) Laser and Fiber Positioning

Precise, stable and independent laser and fiber motions are absolutely essential. The present system allows translation precision as follows:

Laser	x,y motions to 1 μm
Fiber	x motions to 25.4 μm y,z motions to 0.25 μm

Also a rotation stage was added to allow laser rotation about the optical axis (z) with precision of 60 arc seconds. All motions are controlled with micropositioner screws. Unavoidably the parts vibrate slightly then during translation. Piezoelectrically controlled translation stages for fine adjustments (to 0.1 μm) should be among the first priorities for future improvement of the present system. Furthermore even though all parts are solidly attached by magnetic bases to a one inch thick metal table, the system is sensitive to building vibrations. If possible it would be preferrable to have the complete system attached to an optical bench. Our final measurements were done under "silent building" conditions, i.e., data was collected after dark.

ii) Preparation of the Source

In order to get the fiber close to the source, the laser window

(or entire cap) must be carefully removed and the laser chip must be mounted on the edge of the copper base. This requires a special order to the manufacturer. Even then, laser chips are normally placed on the order of 10 μm behind the edge. A very delicate and laborious procedure must then be performed with a steel scalpel blade, micro-positioning screws and microscopes in order to reduce the region of copper base on which the laser sits without damaging the GaAs chip. This work has been performed successfully in our laboratory, although the laser response was unavoidably slightly degraded. It would be highly desirable to obtain directly from the manufacturer uncapped lasers overhanging the copper block.

iii) Laser Response and Stability

Ideally the laser should be operated in the linear lasing region of its response, at an injection at least 10% above threshold to insure high lasing to fluorescent power ratio. This requires the laser to respond linearly to currents at least 12% higher than threshold. Unfortunately our laser did not have such a dynamic range (see Figure 4-4). Experience has further shown that for our purposes injection currents should be regulated and controlled to 0.1%. Our present system regulates and allows readings with an accuracy of only 1%.

iv) Laser Supply Transients

Most regular power supplies upon turning "on" or "off" may produce a transient a few microseconds long and of enough peak current to damage the laser. These transients are due to a sudden change in line

current at the input transformer. This, until detected, was one of our most serious problems. Unfortunately after the damage the laser still operates as a highly radiant LED. Its original response curve however, if known, will be seen to have suffered a dramatic alteration. Threshold is no longer as clearly determined.

A solid state relay circuit was designed for our power supply to prevent the transients when switching the supply "on" or "off." However, transients may still occur if the system is unplugged or the 110 v. feeder accidentally turned off while the power supply is on. The present laser power supply should be redesigned to completely eliminate the possibility of laser damage due to transients.

5. CONCLUSION

The optical properties of single-mode rectangular fibers have been studied with the aim of improving past laser/fiber coupling efficiency results.

Sets of single-mode rectangular fibers were pulled at the Ceramic Engineering Department of this University, and classified for studying. A method of general applicability was developed to measure core dimensions and numerical aperture of fibers. Finally, coupling efficiency measurements were performed by a more reliable procedure for differentiating cladding from core output power than what has been generally used. Our best results have yielded efficiency values of the order of 30%, with a maximum of 50%. If laser fluorescent power is subtracted in order to compare with other published results, the above figures become 46% and 71% respectively. Alignment tolerances are however critical.

The aim of any future work should now be to:

i) Improve the fiber fabrication process in order to decrease transmission losses and achieve better control over the NA value of the final fiber.

ii) Study and optimize the overall laser/transition fiber/round single-mode fiber coupling efficiency.

For this purpose a brief discussion of the main experimental difficulties as well as a group of highly recommended improvements on the present system have been included with the hope of assisting and encouraging future research in this area.

REFERENCES

1. Hsu, H. P. and W. S. C. Chang, "Coupling Methods in Prospective Single-Mode Fiber Integrated Optics Systems: A Progress Report," Fiber and Integrated Optics, Vol. 1, p. 153, 1977.

2. Panish, M. B., "Heterostructure Injection Lasers," Proc. IEEE, Vol. 64, p. 1512, 1976.

3. Cohen, L. G., "Power Coupling from GaAs Injection Lasers into Optical Fibers," Bell Syst. Tech. J., Vol. 51, p. 573, 1972.

4. Boivin, L. P., "Thin-Film Laser-to-Fiber Coupler," Appl. Opt., Vol. 13, p. 391, 1974.

5. Cohen, L. G. and M. V. Schneider, "Microlenses for Coupling Optical Fibers to Junction Lasers," J. Opt. Soc. Am., Vol. 63, p. 1294, 1973.

6. Weidel, E., "Light Coupling From a Junction Laser into a Monomode Fibre with a Glass Cylindrical Lens on the Fiber End," Opt. Commun., Vol. 12, p. 93, 1974.

7. Weidel, E., "New Coupling Method for GaAs Laser-Fibre Coupling," Electron. Lett., Vol 11, p. 436, 1975.

8. Dalgoutte, D. G., G. L. Mitchell, R. L. K. Matsumoto, and W. D. Scott, "Transition Waveguides for Coupling Fibers to Semiconductor Lasers," Appl. Phys. Lett., Vol. 27, p. 125, 1975.

9. Jackson, J. D., Classical Electrodynamics, 2nd Ed., New York: Wiley, 1975, Chapter 6.

10. Ishimaru, A., "Notes on Complex Waves," Electrical Engineering, University of Washington, Seattle, WA. Unpublished work.

11. Mitchell, G. L. and W. D. Scott, "Optical Fiber Cutting Machine for Rectangular and Circular Fibers," 1977, AD-A041 506, available from National Tech. Information Service, Springfield, VA.

12. Yariv, A., Introduction to Optical Electronics, 2nd Ed., New York: Holt, Rinehart and Winston, 1976, Sec. 6.5.

13. Ibid., Chapter 4.

14. Marcuse, D., Light Transmission Optics, Bell Lab. Series, Van Nostrand Reinhold, 1972, Chapter 6.

15. Carlson, F. P., Introduction to Applied Optics for Engineers, New York: Academic Press, 1977, Chapter 2.

16. Popov, Yu. M. and N. N. Shuikin, "Calculation of the Matching of an Injection Laser to a Dielectric Waveguide," Sov. J. Quant. Electron., Vol. 4, p. 986, 1975.

17. Clarricoats, P. J. and A. B. Sharpe, "Modal Matching Applied to a Discontinuity in a Planar Surface Waveguide," Electron. Lett., Vol. 8, p. 28, 1971.

18. Smith, R. B. and G. L. Mitchell, "Analysis of Coupling Efficiency Between Semiconductor Lasers and Rectangular Dielectric Waveguides," 1975, AD-A016 619, available from National Tech. Information Service, Springfield, VA.